mater.scichina.com link.springer.com

Published online 13 May 2024 | https://doi.org/10.1007/s40843-024-2900-5
Sci China Mater 2024, 67(6): 1740–1764

SPECIAL TOPIC: Advanced Energy Catalytic Materials

Progress and challenges of photocatalytic reduction of CO_2 with g-C_3N_4-based photocatalysts in the context of carbon neutrality

Haiyin Zhan[1], Ruiren Zhou[2], Kewang Liu[1], Zhihui Ma[1], Pengfei Wang[1], Sihui Zhan[1] and Qixing Zhou[1*]

ABSTRACT **Global warming has seriously threatened the industrial/agricultural productions and human life and has become one of the major challenges facing the world today. Carbon neutrality is an important measure for mitigating the greenhouse effect, and photocatalytic CO_2 reduction can effectively reduce carbon emissions and promote the carbon cycle. g-C_3N_4 has attracted much attention due to its simple preparation process, high stability, suitable energy band position, and excellent photocatalytic performance; thus, improving its efficiency in photocatalytic CO_2 reduction has become the focus of current research. The importance of carbon neutrality for the global ecological balance and environmental sustainability and the important role and development prospects of g-C_3N_4 photocatalytic CO_2 reduction in the context of carbon neutrality are the main focuses of this review. The current methods and technical means to solve the difficulty of the g-C_3N_4 photocatalytic CO_2 reduction are summarized. The possible problems in the field of g-C_3N_4 photocatalytic CO_2 reduction are discussed, and future research directions are proposed. The aim of this work is to provide theoretical support for the practical applications of g-C_3N_4 photocatalytic CO_2 reduction and to present potential design concepts for efficient g-C_3N_4-based photocatalysts.**

Keywords: carbon neutral, photocatalysis, CO_2 reduction, graphitic carbon nitride, modification strategy

INTRODUCTION

Global warming has seriously threatened the productivity of humans and has become one of the major challenges facing the world today. Global warming is caused by the continuous emissions of carbon dioxide (CO_2), methane (CH_4), ozone (O_3) and other greenhouse gases that produce the greenhouse effect; thus, the temperature continues to rise. Global warming has catastrophic impacts on the earth and production life on which human depends and is a common concern of all countries and governments around the world. CO_2, as the main greenhouse gas, is an important medium of the global carbon cycle and has the dual properties of transforming organic matter in the ecosystem and causing the greenhouse effect [1]. To address climate change caused by the greenhouse effect, the Paris Agreement and the Intergovernmental Panel on Climate Change (IPCC) took the lead in proposing the goal and concept of carbon neutrality in 2015 [2]. In the context of the global climate change and carbon neutrality, CO_2 reduction and conversion have become inevitable trends and choices for green development. Carbon capture and CO_2 conversion and utilization have become key areas of research; additionally, technologies need to be developed urgently and include the development of low-carbon energy, low-carbon transformation of industrial enterprises, low-carbon transformation of domestic energy use, low-carbon transformation of transportation and travel, and the capture and transformation of unavoidable CO_2 emissions [3,4]. Among them, the catalytic reduction of CO_2 to methanol (CH_3OH), CH_4 and other fuels for reuse under the action of catalysts is a key step in achieving carbon neutrality as well as mitigating the greenhouse effect and energy crisis; this reduction is one of the most direct and effective measures for promoting carbon neutrality.

After decades of research, the more mature CO_2 reduction technologies include electrocatalytic reduction, photocatalytic reduction, bioreduction, chemical reduction, reforming reduction and inorganic reduction [5,6]. The recent studies have focused mainly on the electrocatalytic reduction and photocatalytic reduction of CO_2 because of their great potentials in the reduction of CO_2 into other chemicals. Electrocatalytic CO_2 reduction is considered to be an effective strategy; here, electrical energy is stored during the electrocatalytic CO_2 reduction reaction by the reorganization of the molecular bonds between CO_2 and water to form oxygen and CO_2 reduction products [7]. Although the mechanism of the electrocatalytic CO_2 reduction reaction is relatively understood after years of exploration, some problems still remain in the electrocatalytic reduction of CO_2, including the need for electrical energy consumption, unstable reaction kinetics, low energy efficiency, and poor selectivity. Due to these problems, its practical application has been limited [8]. The reduction of CO_2 to chemicals using solar photocatalysis is considered a green and sustainable process; for example, in artificial photosynthesis, CO_2 is converted to various hydrocarbon fuels, such as CH_4, formaldehyde (HCHO), CH_3OH, and formic acid (HCOOH), and this reaction is driven by the renewable solar energy in the presence of a catalyst at ambient temperature and pressure [9]. This is considered a promising

[1] Ministry of Education Key Laboratory of Pollution Processes and Environmental Criteria, Carbon Neutrality Interdisciplinary Science Centre/College of Environmental Science and Engineering, Nankai University, Tianjin 300350, China
[2] Department of Biological and Agricultural Engineering, Texas A&M University, 126 Hobgood, 2117 TAMU, College Station, TX 77843-2117, USA
[*] Corresponding author (email: zhouqx@nankai.edu.cn)

technology for CO_2 reduction and carbon cycling in the context of carbon neutrality because it is green and environmentally friendly and does not consume other energy sources. The efficiency of photocatalytic CO_2 reduction depends mainly on the photocatalysts, and several types of photocatalysts have been developed, including metal oxides (TiO_2 [9,10], CuO/Cu_2O [11], CeO_2 [12,13], ZnO [14], WO_3 [15], In_2O_3 [16], Bi_2WO_6 [17], etc.), nonmetallic semiconductors (g-C_3N_4 [18,19], graphene oxide (GO) [20,21], boron nitride (BN) [22], etc.), and metal organic frameworks (MOFs) [23–25].

Among these photocatalysts, g-C_3N_4 has attracted much attention due to its low cost, simple preparation process, high stability, suitable energy band position and excellent photocatalytic performance. g-C_3N_4 was first reported by Wang *et al.* [26] in 2009 for visible light photocatalytic cracking of water, and g-C_3N_4 was formally applied to the field of catalysis. With an optical band gap of approximately 2.7 eV, g-C_3N_4 is a good visible light responsive material, and its conduction band (CB) and valence band (VB) have energy positions of −1.1 and 1.6 eV relative to the normal hydrogen electrodes (NHEs), respectively. Because of its suitable CB and VB and good stability, g-C_3N_4 is widely used for photocatalytic pollutant degradation, photocatalytic water splitting, photocatalytic CO_2 reduction and so on. For photocatalytic CO_2 reduction, the redox potential of the CO_2 reduction product is generally between −0.16 and −0.62 eV relative to the standard hydrogen electrode. The bottom of the CB of g-C_3N_4 is more negative with respect to the redox potential of the CO_2 reduction products, which provides the necessary conditions for the catalytic reaction [27,28]. However, the low utilization efficiency of g-C_3N_4 for sunlight limits its practical application in photocatalytic CO_2 reduction, mainly due to the fast electron and hole recombination rate (low electron utilization) of pure g-C_3N_4 and the low absorption efficiency of visible light. To overcome the above disadvantages in enhancing the efficiency of photocatalytic CO_2 reduction, various modulation methods, such as heterostructure building, elemental doping, and noble metal deposition, have been studied and reported. These modulation methods provide more possibilities for the practical applications of g-C_3N_4 in photocatalytic CO_2 reduction.

Herein, we focus on the importance of carbon neutrality for global ecological and environmental sustainability and the important role and development prospects of g-C_3N_4 photocatalytic CO_2 reduction in the context of carbon neutrality. First, a basic understanding of carbon neutrality and the basic principles of g-C_3N_4 photocatalytic CO_2 are introduced. Second, the current methods and technical means to solve the difficulties limiting g-C_3N_4 photocatalytic CO_2 reduction are reviewed. Finally, the possible future problems of g-C_3N_4 in the field of photocatalytic CO_2 reduction are discussed, and future research directions are presented. This review aims to provide theoretical support for the applications of g-C_3N_4 photocatalytic CO_2 reduction in a carbon-neutral environment and provides suggestions for promoting the practical applications of g-C_3N_4 photocatalytic CO_2 reduction and the design of efficient g-C_3N_4-based photocatalysts.

SIGNIFICANCE AND NECESSITY OF CARBON NEUTRALITY

With the development of human civilization and the global economy, climate change has become the most important issue facing humanity today. Due to global warming, we are experiencing a series of catastrophic weather and climate events, such as heat waves, floods, droughts, forest fires and sea level rise. Global warming is caused by the massive use of fossil fuel energy by humans since the industrial revolution, the massive amounts of manufacturing, housing infrastructure, and other activities; these activities have resulted in the emission of large amounts of greenhouse gases (mainly CO_2 but also CH_4, nitrous oxide, and chlorofluorocarbons), which are commonly called carbon emissions. To limit the harm of global warming, global carbon emissions need to be rapidly reduced. Carbon neutrality, also known as carbon offset, is an inevitable option that can reduce global warming in response to climate change. The concept of carbon neutrality was first proposed by environmentalists in the late 1990s, and the global and national carbon neutrality targets originated from the 2015 Paris Agreement on climate change and the relevant reports of the IPCC [29]. Carbon neutrality means that the total amount of carbon dioxide or greenhouse gas emissions generated directly or indirectly by a country, enterprise, product, activity or individual over a certain period of time can be offset through afforestation, energy conservation and emission reduction to achieve a positive or negative offset and attain relative "zero emissions" [30]. An important point in the process of carbon neutrality is peak emissions, also known as carbon peaking, which refers to a point in time when CO_2 emissions stop increasing, reach a peak and then gradually decrease and is the turning point of CO_2 emissions from increasing to decreasing. The goals set out in the Paris Agreement require parties to the United Nations Framework Convention on Climate Change are as follows: to make immediate and explicit intended nationally determined contributions (INDCs) to climate change mitigation; to peak carbon emissions as early as possible; to achieve carbon neutrality in the second half of the 21st century; and to limit the increase in global surface temperature to 2°C relative to preindustrial levels by the end of the 21st century; this effort would move towards the control target temperature of 1.5°C [31,32].

In this dire situation, future greenhouse gas emission limits will be extremely stringent in the longer term. In a special report in 2018, the IPCC stated that countries must achieve "net zero" CO_2 emissions by 2050 to maintain global warming within 1.5°C of preindustrial levels [33]. However, to maintain temperatures within 2°C at minimal cost, scientific studies have found that global greenhouse gas emissions need to peak by 2020. Figueres *et al.* [34] argued that the emission pathway limits the average carbon balance to 600 Gt CO_2; this is consistent with limiting warming to 1.5–2°C. They noted that increasing the emissions budget to 800 Gt CO_2 while still peaking in 2020 would reduce the need for high decarbonization rates after the peak but would increase the risk of temperature increases beyond the 1.5–2°C target (Fig. 1a). Fig. 1b shows the median values for various studies' assessments of anticipated emissions levels in 2025 and 2030 based on the INDCs; these assessments are in contrast with what is needed for limiting warming to 1.5 or 2°C and indicate continuous growth, on average, in emissions between 2025 and 2030 [35].

To combat climate change and achieve the carbon neutrality goals envisioned in the Paris Agreement, governments should actively set carbon neutrality targets and pursue a range of related policies. Socioeconomic, energy and industrial systems as well as individual consumption behaviour will need to be sig-

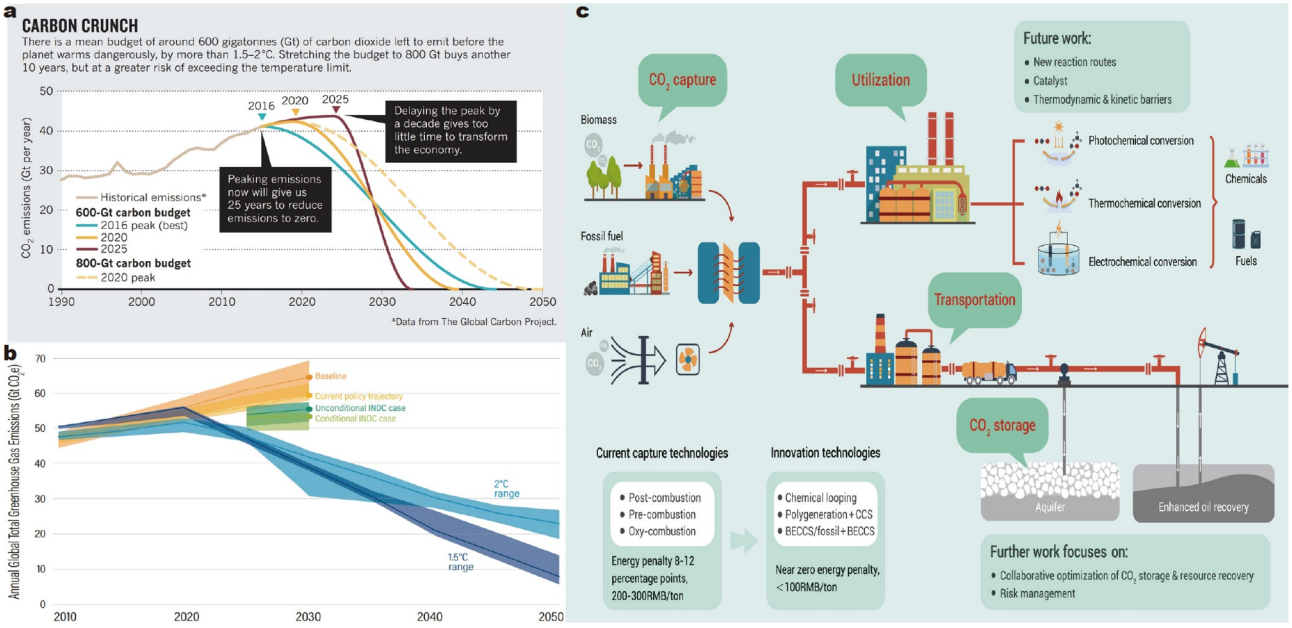

Figure 1 (a) Implications of delay in global emissions peaking on future decarbonization rates needed to stay within 1.5–2°C goal. Reprinted with permission from Ref. [34]. Copyright 2017, Springer Nature. (b) Anticipated emissions levels in 2025 and 2030 with INDCs compared with a 1.5 or 2°C emissions trajectory. Reprinted with permission from Ref. [35]. Copyright 2017, World Resources Institute. (c) The roadmap for CO_2 capture technology development in the industry. Reprinted with permission from Ref. [2]. Copyright 2021, Elsevier.

nificantly rebuilt. The realization of the vision of carbon neutrality requires a combination of policies and the development of relevant emission reduction and sequestration technologies from two main aspects: energy efficiency and carbon capture (Fig. 1c) [2,3]. In terms of energy conservation and emission reduction, emerging technologies and technological innovation have become important tools for promoting energy conservation and emission reduction [36]. At present, the technologies used to achieve carbon neutrality mainly include renewable energy technology, low carbon utilization and energy efficiency improvement technology, carbon capture, and utilization and storage (CCUS) technology. Renewable energy is a complete technology system that needs not only solar energy, wind energy, geothermal energy, and ocean energy but also the cooperation of energy storage technology to form a new energy system. Nuclear energy and hydrogen energy have the advantages of being clean, low-carbon, green and environmentally friendly and are important technologies for achieving carbon neutrality. Low carbon use and energy efficiency technologies are mainly applied in industry, transportation and buildings. These include the following: clean and efficient utilization technology of coal, oil and natural gas; low carbon and zero carbon industrial process reengineering technology; electrification and intelligent transportation technology; and direct and flexible light storage to build photovoltaic integration technology systems. CCUS technology mainly includes carbon dioxide into chemicals, carbon dioxide into fuel, microalgae production, concrete carbon capture, carbon capture and storage of bioenergy, afforestation [2,37,38]. In addition, effective policies, such as launching low-carbon pilot projects, promoting "green markets", need to be implemented, and carbon emission trading market mechanisms need to be established [39]. However, the total emissions from aviation, long-distance transport, shipping, structural materials, and highly reliable electricity that are difficult to eliminate are approximately 920 million tons of CO_2, accounting for 27% of the global CO_2 emissions from all fossil fuels at that time (2014) (Fig. 2a) [40,41]. Therefore, the development of carbon sequestration technologies capable of capturing and converting CO_2 is particularly important in the process of achieving carbon neutrality, and photocatalytic CO_2 reduction as artificial photosynthesis can effectively contribute to the carbon cycle and reduce CO_2 emissions (Fig. 2b–d) [42–44]. As shown in Fig. 2e, g-C_3N_4 has the most suitable energy band position among many common photocatalysts and can meet the redox potential of most reactions. Therefore, it has broad prospects and research significance in the field of photocatalytic CO_2 reduction. The process of achieving carbon neutrality requires long-term effort, and technological innovation is the key to achieving carbon neutrality. In today's rapid economic development, achieving carbon neutrality has become a development initiative, and the attainment of carbon neutrality has great and long-term value for human survival and development.

BASIC PRINCIPLE OF g-C_3N_4 PHOTOCATALYTIC REDUCTION OF CO_2

Basic principle and thermodynamic study of photocatalytic CO_2 reduction

Photocatalytic technology uses renewable solar energy as the only energy source and semiconductors with suitable energy band locations as catalysts to transform light energy into chemical energy to cause the oxidation and reduction reactions of various substances; thus, environmental remediation and material circulation can be attained with the characteristics of high efficiency, environmental friendliness and economy [45]. In early 1979, Inoue and colleagues [46] first reported the photocatalytic reduction of CO_2 to form organic compounds such as HCHO, HCOOH, CH_3OH, and CH_4 in the presence of a

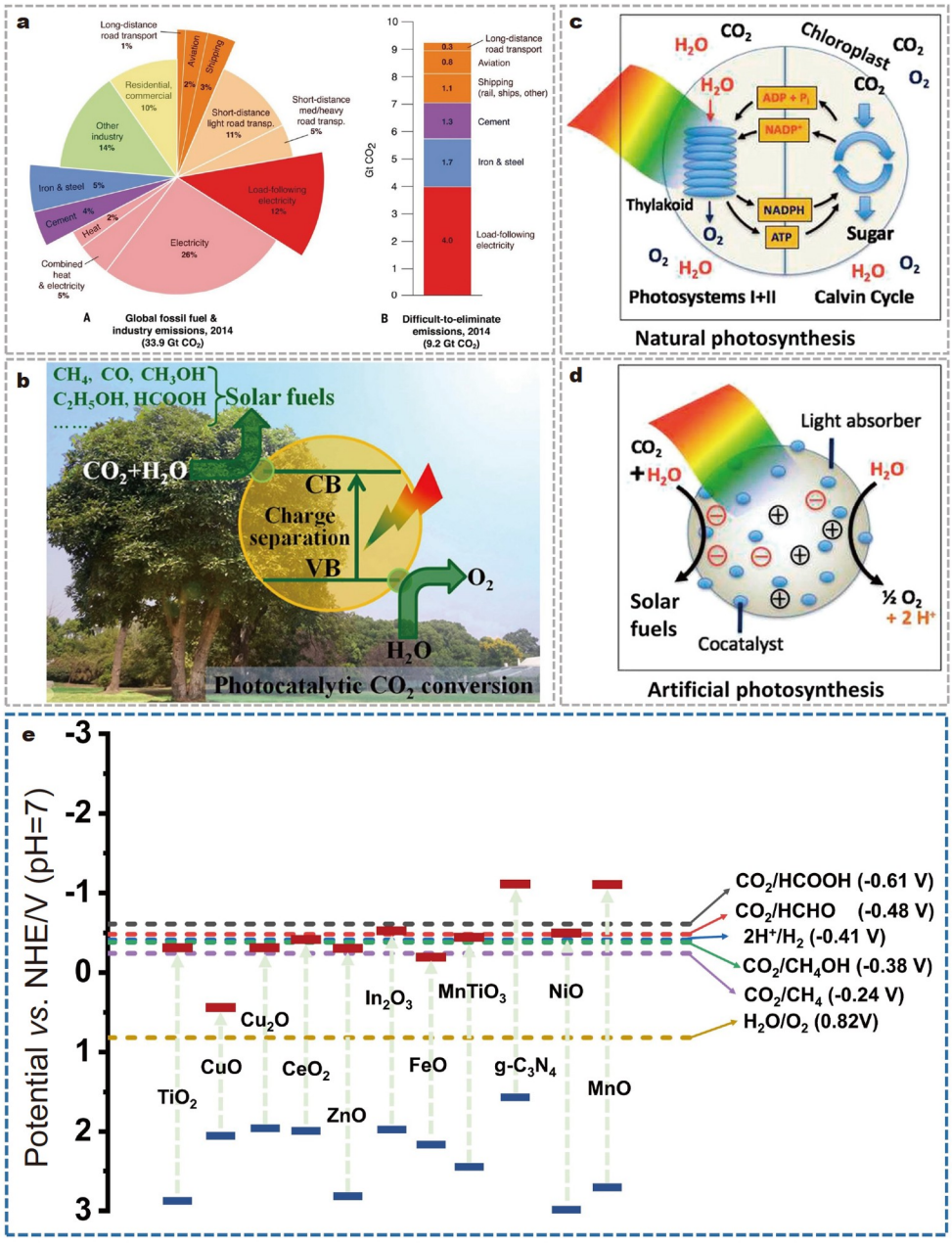

Figure 2 (a) Difficult-to-eliminate emissions in current context. Reprinted with permission from Ref. [40]. Copyright 2018, American Association for the Advancement of Science. (b) Mechanism of photocatalytic reduction of CO_2 on semiconductors. Reprinted with permission from Ref. [43]. Copyright 2016, American Chemical Society. Schematic illustrations for natural (c) and artificial (d) photosyntheses. Reprinted with permission from Ref. [44]. Copyright 2017, American Chemical Society. (e) Comparison of band positions of common photocatalysts with redox potentials of different products generated by photocatalytic CO_2 reduction.

semiconductor powder suspended in water as a catalyst. Since then, researchers have been interested in the photocatalytic CO_2 reduction in semiconductors. The photocatalytic activity of semiconductor catalysts is produced by their special energy band structure. Semiconductor catalysts are usually composed of the following: a low-energy VB, which is occupied by electrons; a high-energy CB, which is not occupied by electrons; and a band gap. When the sun shines on the surface of the semiconductor, the semiconductor absorbs the energy of the photon, and when the energy of the photon is greater than or equal to the bandgap energy (bandgap width) of the semiconductor, the electrons in the VB will be excited to transition to the CB, leaving relatively stable holes in the VB, thus forming an electron-hole pair. Subsequently, the electron-hole migration to the surface of the catalyst and the substances adsorbed on the surface of the catalyst cause reduction and oxidation reactions, thus achieving environmental remediation or material cycling (Fig. 3a) [47]. In a typical photocatalytic reaction, there are four key steps: (1) adsorption of reactants on the catalyst surface; (2) light excitation production of e-h^+ pairs; (3) separation and migration of e-h^+ pairs; and (4) oxidation and reduction reactions on the catalyst surface. Therefore, the number of adsorption sites (reaction sites) on the catalyst surface, the absorption efficiency of sunlight, the separation efficiency of e-h^+ pairs and the

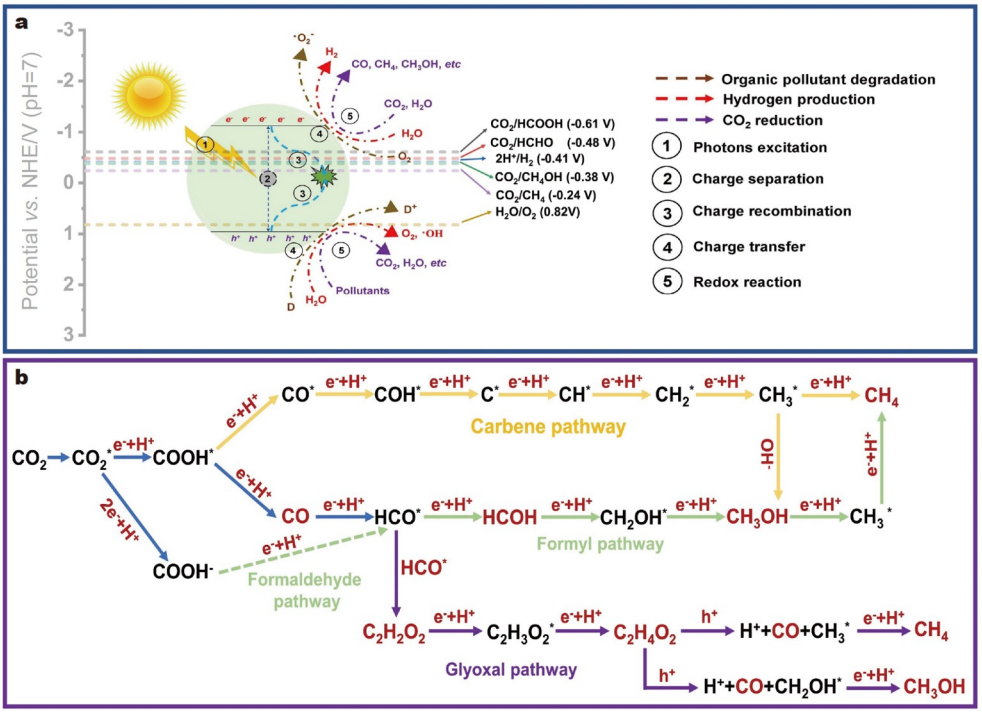

Figure 3 (a) Schematic diagram of the basic principles of photocatalysis. Reprinted with permission from Ref. [47]. Copyright 2022, Elsevier. (b) Reaction pathways for photocatalytic CO_2 reduction of common products [53]. Copyright 2022, American Chemical Society.

appropriate energy band structure are crucial to the efficiency of the photocatalytic reaction [48,49].

Driven by sunlight, the use of photocatalytic materials to catalyse the conversion of CO_2 into renewable hydrocarbon fuel at room temperature and pressure to achieve CO_2 reduction and carbon recycling is considered to be the most environmentally friendly and effective way to mitigate the greenhouse effect and alleviate the energy crisis. CO_2, the most common greenhouse gas, is linearly connected between carbon and oxygen atoms by two C=O bonds with a C=O bond energy of up to 750 kJ mol^{-1} [27]; this energy is much greater than the energy required to split C–C, C–O, and C–H bonds, and the C=O bond is one of the most thermodynamically stable carbon compounds (ΔG_f^o = −394.39 kJ mol^{-1}) [50]. If CO_2 reduction is achieved, sufficient energy is needed to break the C=O bond; thus, its conversion into valuable chemicals without a catalyst and sufficient energy is almost impossible to achieve. In addition, CO_2 has a high band gap of approximately 13.7 eV between its highest occupied molecular orbital (HOMO) and lowest unoccupied molecular orbital (LUMO) with a large electron affinity (−0.6 ± 0.2 eV); thus, it is considered to be an inactive molecule [51]. Due to its inactivity, the one-electron reaction produces a negative redox potential (Equation (1) *vs.* NHE at pH 7), which is thermodynamically unfavourable for the reaction [52]. In contrast, for the CO_2 reduction reaction to be carried out more easily, bypassing the formation of $\cdot CO_2^-$ by using a proton-assisted multielectron reduction step with a lower redox potential might be more thermodynamically advantageous, and this depends on the number of protons involved and the number of electrons transferred. CO_2 can be reduced to different fuels and chemicals, such as HCOOH, CO, HCHO, CH_3OH, and CH_4 (Equations (2)–(6) *vs.* NHE at pH 7) [43,52].

$$CO_2 + e^- \rightarrow CO_2^{-\bullet},\ E_0 = -1.90\ \text{eV}, \quad (1)$$

$$CO_2 + 2H^+ + 2e^- \rightarrow HCOOH,\ E_0 = -0.61\ \text{eV}, \quad (2)$$

$$CO_2 + 2H^+ + 2e^- \rightarrow CO + H_2O,\ E_0 = -0.53\ \text{eV}, \quad (3)$$

$$CO_2 + 4H^+ + 4e^- \rightarrow HCHO + H_2O,\ E_0 = -0.48\ \text{eV}, \quad (4)$$

$$CO_2 + 6H^+ + 6e^- \rightarrow CH_3OH + H_2O,\ E_0 = -0.38\ \text{eV}, \quad (5)$$

$$CO_2 + 8H^+ + 8e^- \rightarrow CH_4 + 2H_2O,\ E_0 = -0.24\ \text{eV}. \quad (6)$$

The formation path of photocatalytic CO_2 reduction products is shown in Fig. 3b, and its reaction pathways mainly include the carbene pathway, formyl pathway, and glyoxal pathway [53–56]. The smooth progress of the photocatalytic CO_2 reduction reaction must meet the basic thermodynamic requirements. In simple terms, the position at the bottom of the CB must be more negative than the redox potential of CO_2 to ensure that the CO_2 reduction reaction has sufficient driving force. The position of the top of the VB should be more corrected than the redox potential of H_2O to produce protons and consume holes. Otherwise, the accumulated holes may be annihilated by the photogenerated electrons, or they can react with the reduction products of carbon dioxide [57]. The adsorption of CO_2 molecules on the surface of a photocatalyst changes its molecular structure from a linear structure to a curved structure. When the O–C–O bond angle of CO_2 molecules decreases from 180°, the LUMO energy of CO_2 decreases, thereby reducing its reaction barrier and promoting the CO_2 reduction reaction [58,59].

Principle of g-C_3N_4 photocatalytic reduction of CO_2

Among various photocatalysts, g-C_3N_4 is a promising photocatalyst for CO_2 reduction. As early as 1922, Franklin [60] introduced the concept of "carbonic nitride" (C_3N_4) and suggested that C_3N_4 might be obtained as the final deamination product of a series of ammono-carbonic acids by heating melon [61]. Later, Pauling and Sturdivant [62] clarified that the basic structural unit of carbon nitride and its derivatives was the coplanar tri-*s*-triazine ring. After years of research, C_3N_4 was

found to mainly include five different structures: α-C_3N_4, β-C_3N_4, cubic C_3N_4, pseudo-C_3N_4 and graphitic C_3N_4 (g-C_3N_4) [63]. Among them, g-C_3N_4 is a metal-free mid-bandgap P-type semiconductor with reliable chemical and thermal stability; thus, it is very popular in photocatalyst research. g-C_3N_4 can be synthesized by the thermal condensation of various nitrogen-rich precursors, such as melamine [64–66], dicyandiamide [67,68], cyanamide [69], urea [70,71], and thiourea [72]. The sp^2 hybridization of carbon and nitrogen atoms in g-C_3N_4 results in the formation of a highly delocalized π-conjugated system, producing a suitable band gap for visible light photocatalytic reactions of approximately 2.7 eV [73]. Notably, the CB position of g-C_3N_4 at approximately −1.1 eV and the VB position at approximately 1.6 eV (relative to NHE) are ideal band positions for most photocatalytic reactions, including CO_2 reduction [50]. The basic structure, physical and chemical properties of g-C_3N_4 and the basic principle of photocatalysis have been reviewed by many scholars [74–82]; thus, here, we focus on the basic principle and application of g-C_3N_4 in the field of photocatalytic CO_2 reduction.

The outstanding performance of g-C_3N_4 in the field of photocatalytic CO_2 reduction has prompted researchers to explore and uncover its reduction mechanism. Furthermore, the photocatalytic reduction process of CO_2 on g-C_3N_4 is a typical semiconductor catalyst-led photocatalytic CO_2 reduction process, and its basic reaction process is consistent with the reaction mechanism mentioned above. The adsorption and activation of CO_2 on a catalyst surface is a critical and challenging step in the CO_2 photoreduction process and is used to determine the photocatalytic CO_2 reduction rate and product selectivity [83]. Compared with normal CO_2 molecules, CO_2 in the chemisorbed state (mainly carbonate and/or CO_2^- anion) has a bent O–C–O bond angle, and its LUMO is reduced; this facilitates charge transfer from the photoexcited semiconductor to the surface-adsorbed CO_2 molecules [43]. Generally, the adsorption of CO_2 molecules by atoms on the surface of semiconductor catalysts mainly includes three situations [84]: O of CO_2 is separately adsorbed on the acidic surface atom of the catalyst (Fig. 4a), C of CO_2 is separately adsorbed on the basic surface atom of the catalyst (Fig. 4b), and the C and O atoms of CO_2 are mixed adsorbed on the surface of the catalyst (Fig. 4c). g-C_3N_4 is prone to interactions with the C atom of the acid CO_2 gas (a Lewis acid) due to the presence of lone electron pairs on the Lewis base at the N atomic site on its surface [85]. There are two main adsorption modes of CO_2 on the surface of g-C_3N_4 molecules: vertical adsorption and parallel adsorption. According to the density functional theory (DFT) calculations by Zhu *et al.* [86], the adsorption of CO_2 on the surface of g-C_3N_4 was more prone to parallel adsorption, and the doubly coordinated N atom was the main adsorption site, with a maximum adsorption energy of −0.42 eV. In addition, their study also showed that g-C_3N_4 showed a strong adsorption capacity for CO_2 and H_2O (E_{Ads} greater than −0.30 eV), while the adsorption strength for CO and CH_4 was weak (E_{Ads} less than −0.163 eV). Fortunately, CO_2 and H_2O were the reactants of the CO_2 photocatalytic reduction. In contrast, CO and CH_4 were products of CO_2 photocatalytic reduction. Therefore, the adsorption behaviour of g-C_3N_4 was characterized by high adsorption of reactants and weak adsorption of products; this behaviour is very favourable for the photocatalytic reaction process [86]. However, most studies believe that the adsorption of CO_2 on the surface of g-C_3N_4 is mainly physical adsorption process [86–88]. To further improve the efficiency and application prospects of photocatalytic CO_2 reduction, g-C_3N_4 needs to be modified to improve its ability to adsorb and activate CO_2 molecules, and the specific surface area, surface basic groups, increased adsorption sites and edge defects should be considered. Fu *et al.* [66] used continuous thermal oxidation spalling and rolling methods to prepare layered porous g-C_3N_4 nanotubes doped with O. Their results showed that O doping enhanced the adsorption capacity of the catalyst for CO_2, resulting in excellent photocatalytic CO_2 reduction performance under visible light, and the methanol precipitation rate

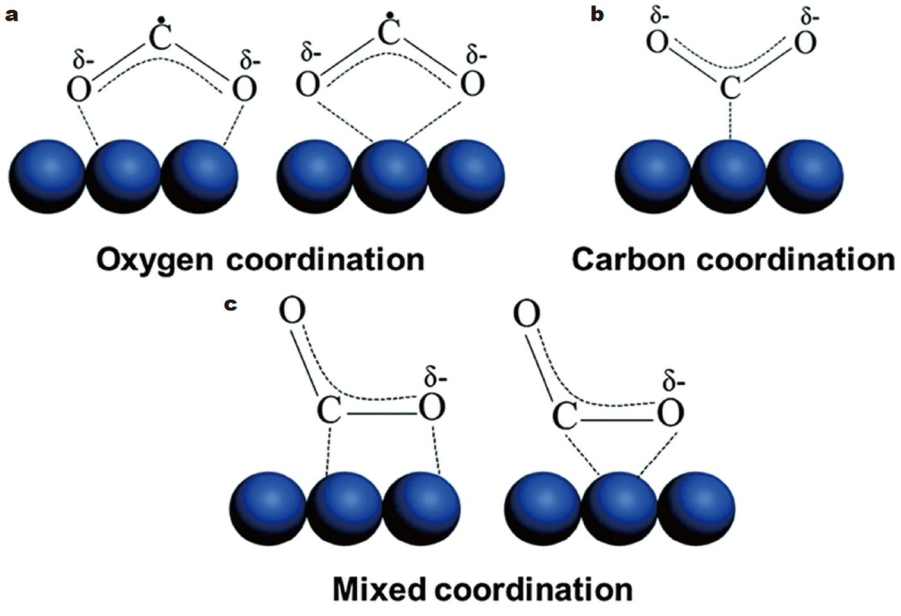

Figure 4 Several configurations of surface atoms adsorbing CO_2 molecules on semiconductor catalysts. Reprinted with permission from Ref. [84]. Copyright 2016, Royal Society of Chemistry.

was 0.88 μmol g^{-1} h^{-1}. This value was five times greater than that of bulk g-C_3N_4 (0.17 μmol g^{-1} h^{-1}).

The photocatalytic activation of CO_2 by g-C_3N_4 depends on its optical and photoelectrochemical properties. Ultraviolet-visible diffuse reflection spectroscopy (UV-vis DRS) can be used to study the light absorption performance of a catalyst. Photoluminescence (PL) spectroscopy can show the separation and migration efficiency of photogenerated carriers after photoexcitation, and the photocurrent response can be used to explain the migration efficiency of photogenerated carriers to the catalyst surface [89]. Chen *et al.* [90] loaded a single La atom on g-C_3N_4 to obtain O/La-CN, and the introduction of La–N bonds promoted the efficiency of the CO_2 reduction reaction. After the single-atom loading of La, the PL intensity of O/La-CN significantly decreased (Fig. 5a), and its light absorption edge redshifted (Fig. 5b), resulting in a significant improvement in its photocatalytic CO_2 reduction efficiency (Fig. 5c). Xu *et al.* [91] successfully constructed a van Der Waals (vdW) heterostructure between the layered Bi_3O_4Cl and two-dimensional (2D) g-C_3N_4 for photocatalytic CO_2 reduction (Fig. 5d). Compared with Bi_3O_4Cl and g-C_3N_4, the photocurrent response intensity of Bi_3O_4Cl/20% g-C_3N_4 was also greatly improved, which indicated that the photoelectron-hole pair separation efficiency was greater after the construction of the vdW heterojunction (Fig. 5e). The PL test showed that Bi_3O_4Cl/20% g-C_3N_4 had the lowest electron and hole recombination efficiency (Fig. 5f). Owing to the good photoelectric performance of the catalyst, the photocatalytic reduction efficiency of CO_2 was significantly improved. g-C_3N_4 is a direct semiconductor with a band gap of 2.7 eV and a corresponding absorption edge of 460 nm. Appropriately reducing the band gap of g-C_3N_4 through heteroatom doping can cause the redshift of the optical absorption edge of the catalyst, effectively improving the optical absorption efficiency and thus improving the efficiency of the g-C_3N_4 photocatalytic reduction of CO_2 [92]. Kim *et al.* [93] introduced Sn and Cu atoms into g-C_3N_4, which reduced the band gap and promoted light absorption (Fig. 5g, h), greatly improving the CO_2 reduction efficiency. Similarly, the absorption edge of sulfur-doped g-C_3N_4 (TCN) showed a redshift of 20 nm compared with that of undoped g-C_3N_4, reaching 475 nm (Fig. 5i). After doping, the band gap decreased from 2.70 to 2.63 eV, indicating that the TCN samples could absorb more solar energy and generate more photogenerated electrons and hole pairs. The yields of CH_3OH from TCN and undoped g-C_3N_4 were 1.12 and

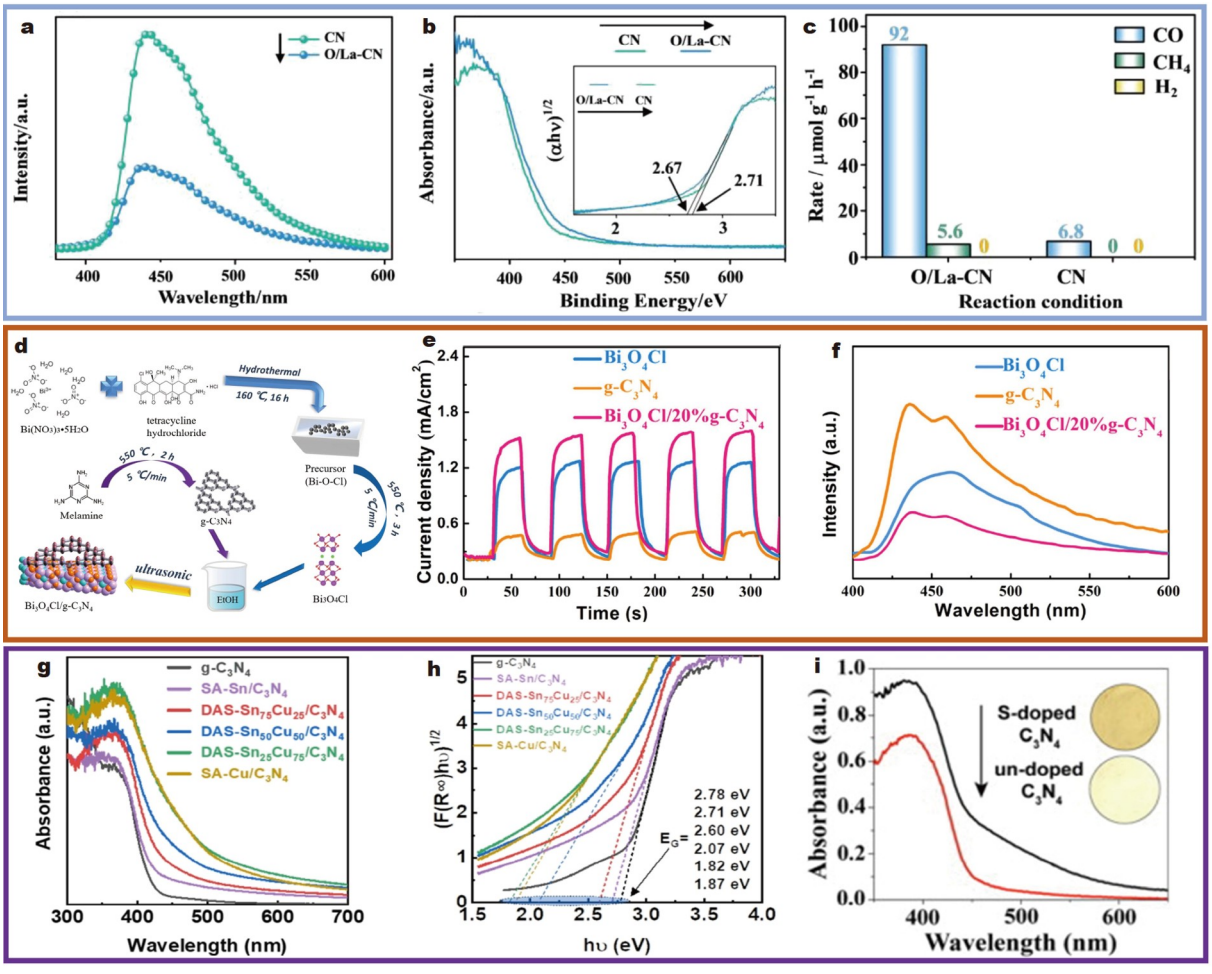

Figure 5 (a) PL spectra, (b) UV–vis DRS spectra and the estimated band gaps and (c) photoreduction rate of CN and O/La-CN. Reprinted with permission from Ref. [90]. Copyright 2020, American Chemical Society. (d) Synthesis process of Bi_3O_4Cl/g-C_3N_4 vdW heterojunction. (e) Electrochemical impedance plots and (f) PL spectra of Bi_3O_4Cl, g-C_3N_4 and Bi_3O_4Cl/20%g-C_3N_4. Reprinted with permission from Ref. [91] Copyright 2021, Elsevier. (g) UV–vis DRS. (h) Optical band-gap determination by DRS. Reprinted with permission from Ref. [93]. Copyright 2023, Wiley. (i) UV–vis DRS and the corresponding colors (inset) of TCN and undoped g-C_3N_4. Reprinted with permission from Ref. [94]. Copyright 2015, Elsevier.

0.81 μmol g^{-1}, respectively [94].

Preliminary studies on photocatalytic CO_2 reduction by g-C_3N_4

g-C_3N_4 is a promising photocatalyst for CO_2 reduction due to its abundant surface functions, highly specific electronic properties and suitable band structure. Goettmann *et al.* [69] showed that using mesoporous graphite carbon nitride (mpg-C_3N_4) as a heterogeneous metal-free catalyst could directly activate carbon dioxide to produce carbamate, which further oxidized benzene to phenol, and the formed CO could be used for subsequent *in situ* reactions (Fig. 6a). They also proposed that the activation of CO_2 adsorbed on the catalyst to form carbamate was considered to be the first step in artificial photosynthesis. Their study was the first attempt to apply g-C_3N_4 in the field of photocatalytic CO_2 reduction, indicating its considerable research potential. Dong and Zhang [95] found that g-C_3N_4 prepared with melamine hydrochloride as the precursor system could effectively photocatalyse the reduction of CO_2 to CO under visible light irradiation in the presence of water vapour and without other assistance. Xia *et al.* [96] showed that crystalline carbon nitride with a surface defect design could efficiently reduce gas-phase CO_2 to hydrocarbon fuel at a rate of 12.07 μmol h^{-1} g^{-1} with a selectivity of 91.5% (Fig. 6b). Studies have shown that in the presence of water vapour, the band structure of the g-C_3N_4 photocatalyst can regulate the selectivity of the CO_2 photoreduction reaction [97]. The main products of CO_2 photoreduction of bulk g-C_3N_4 with a 2.77 eV band gap and g-C_3N_4 nanosheets with a 2.97 eV band gap are CH_3CHO and CH_4, respectively (Fig. 6c). The above study provides a reference for the design of efficient and highly selective photocatalysts for CO_2 reduction from the perspective of the energy band. These early studies demonstrate the potential of g-C_3N_4 in the field of photocatalytic CO_2 reduction and provide theoretical support for further research.

Due to the following advantages, g-C_3N_4 has potential for use in CO_2 reduction reactions. First, its band structure effectively aligns with the oxidation–reduction potentials of CO_2 reduction products. Second, the 2D or multidimensional layered or wrinkled structure of g-C_3N_4 provides more adsorption sites for CO_2 and facilitates the rapid migration of photogenerated electrons to catalytic surface adsorption sites. Third, the band structure of g-C_3N_4 is highly tuneable, enabling the synthesis of g-C_3N_4 with different band structures by using different precursors and synthesis methods. Furthermore, its band structure and optoelectronic properties can be easily modified through elemental doping. However, pristine g-C_3N_4 has several drawbacks that limit its photocatalytic CO_2 reduction efficiency and practical applications. These include a low specific surface area,

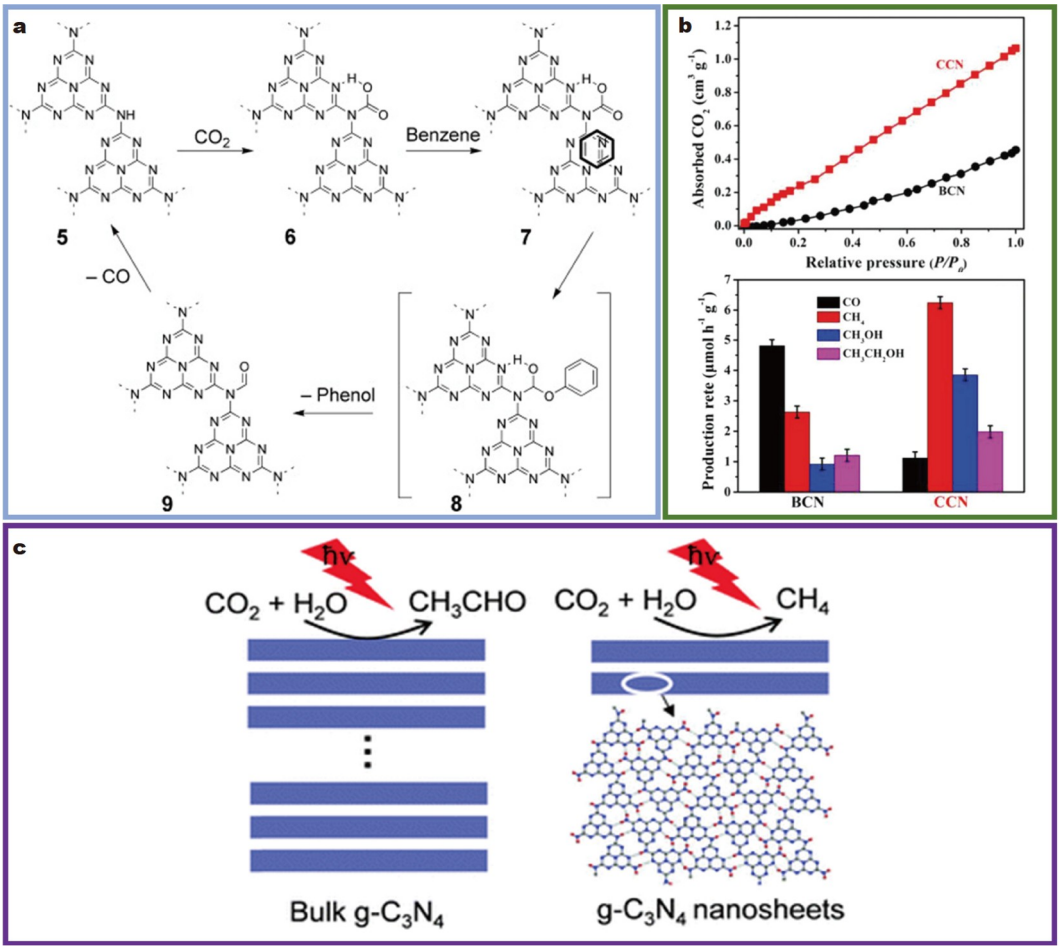

Figure 6 (a) Possible mechanism for the formation of phenol from benzene and CO_2 catalyzed by mpg-C_3N_4. Reprinted with permission from Ref. [69]. Copyright 2007, Wiley. (b) CO_2 adsorption isotherms and photocatalytic CO_2-reduction properties of CCN and BCN. Reprinted with permission from Ref. [96]. Copyright 2023, Wiley. (c) Schematic of the generations of CH_4 and CH_3CHO on bulk g-C_3N_4 and a g-C_3N_4 nanosheets in the photoreduction of CO_2 in the presence of water vapor. Reprinted with permission from Ref. [97]. Copyright 2014, Royal Society of Chemistry.

which hinders CO_2 adsorption, and poor separation of the photogenerated electrons and holes, leading to low photocarrier separation efficiency. Moreover, it exhibits low utilization efficiency for visible light. To overcome these issues and improve photocatalytic efficiency, several strategies have been developed. These strategies aim to enhance CO_2 adsorption, improve the separation and transfer of photogenerated carriers, and extend the light absorption range. These methods include heterojunction construction, elemental doping, and deposition of noble metals, among other modification techniques. These modification strategies provide more possibilities for the practical application of g-C_3N_4 in photocatalytic CO_2 reduction.

SURFACE MODIFICATION IMPROVEMENT IN THE EFFICIENCY OF g-C_3N_4 PHOTOCATALYTIC CO_2

Doping engineering

g-C_3N_4 is a visible light-responsive photocatalyst, with its CB mainly composed of C $2p_z$ orbitals and the N ($2p_x$, $2p_y$) orbitals contributing to its VB. However, the 2.7 eV band gap of g-C_3N_4 restricts its utilization of solar radiation at wavelengths below 460 nm. Generally, the ideal band gap for a semiconductor is approximately 2.0 eV. Therefore, reducing the band gap of g-C_3N_4 can enhance its light absorption properties and provide more photogenerated electrons. Element doping is one of the most commonly used methods to modulate the optical properties and electronic structure of semiconductor photocatalytic materials, providing advantages such as simplicity and high efficiency. By introducing foreign elements into the semiconductor, the charge carrier separation and transfer in the photocatalyst can be facilitated, or the band structure of the semiconductor can be adjusted to improve the light absorption range or match the redox potential of the target reaction. Incorporating suitable elements into g-C_3N_4 can effectively enhance its photocatalytic activity and improve the efficiency of photocatalytic CO_2 reduction. Extensive research has been conducted on enhancing the photocatalytic activity of g-C_3N_4 through metal doping or nonmetal doping.

Metal doping

Metal elements affect the activity and kinetics of photocatalytic reactions mainly by influencing the behaviour of photogenerated carriers in semiconductor photocatalysts. From the point of view of chemical structure, the entry of doped metal atoms into a semiconductor will affect its electronic structure, which will affect the recombination of the photogenerated electrons and holes. For example, when a doped atom becomes a potential well for electrons or holes, it can extend the lifetime of the carrier [98]. In addition to affecting the separation of photogenerated carriers, metal element doping can also expand the optical absorption range of semiconductors because the doped atoms will form new impurity levels in the bandgap of the semiconductor [99]. In general, metal ions (M^{n+}), especially transition metal ions, are doped into large caverns (triangular pores) between connected trinitrogen structures on the g-C_3N_4 plane through strong coordination interactions with negatively charged nitrogen atoms (Fig. 7a); however, alkali metals are more inclined to be doped in the interlayer structure of g-C_3N_4 (Fig. 7b). Fe [100], Cu [101,102], Mo [103], Mg [104], Eu [105], alkali metals (K [68,106], Ca [107], Rb [108]) and other metallic elements have been used to enhance the activity of the g-C_3N_4 photocatalytic reduction of CO_2.

Duan *et al.* [109] doped Cu into g-C_3N_4 to introduce Cu single-atom sites (Fig. 8a, b). The results showed that the Cu single-atom centre promoted the chemisorption and activation of CO_2 through the accumulation of photogenerated electrons, and the $N_{2C}V$ site promoted the dissociation of H_2O, thus promoting the conversion of COO* to COOH*. $Cu_1/N_{2C}V$-CN has a high selectivity (98.50%) and a good CO yield (11.12 μmol g^{-1} h^{-1}) (Fig. 8c). Li *et al.* [110] used different transition metals to modify g-C_3N_4 to obtain MeCN (Me = Cu, Co, Ti, or Fe). The CO evolution rate of the optimized MeCN was significantly greater than that of the undoped g-C_3N_4, in which the Fe-doped g-C_3N_4 showed the highest photocatalytic activity (490 μmol g^{-1} h^{-1}) (Fig. 8d). The increase in the photocatalytic CO_2 reduction activity was attributed to the increase in the catalyst surface area, CO_2 adsorption capacity, visible light absorption, and charge separation and transfer efficiency. Wang *et al.* [106] reported a novel study on potassium-doped g-C_3N_4 (K-CN) for visible light-driven CO_2 reduction. DFT calculations and X-ray photoelectron spectroscopy (XPS) tests indicated that potassium doping occurred between the layers, altering the electronic structure of g-C_3N_4 (Fig. 8e). Under visible light irradiation, K-CN-7 achieved efficient CO_2 reduction without any noble metal cocatalyst, yielding a CO production rate of 8.7 μmol g^{-1} h^{-1}; this value was 25 times greater than that of

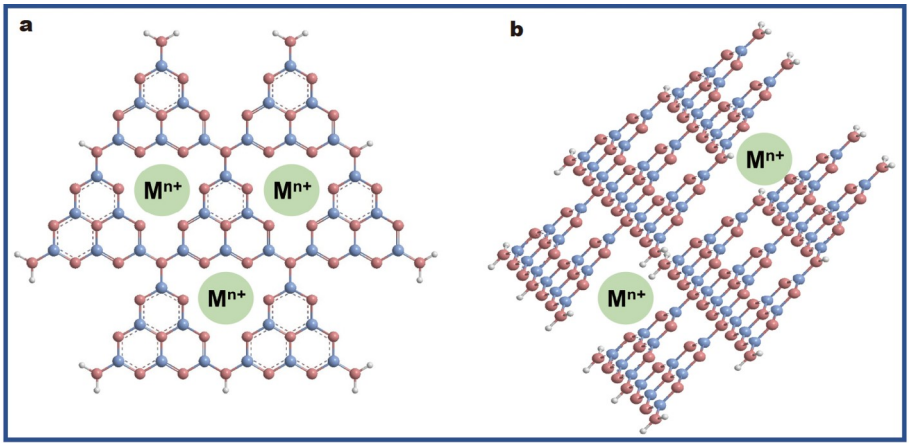

Figure 7 Common locations of metal doped g-C_3N_4.

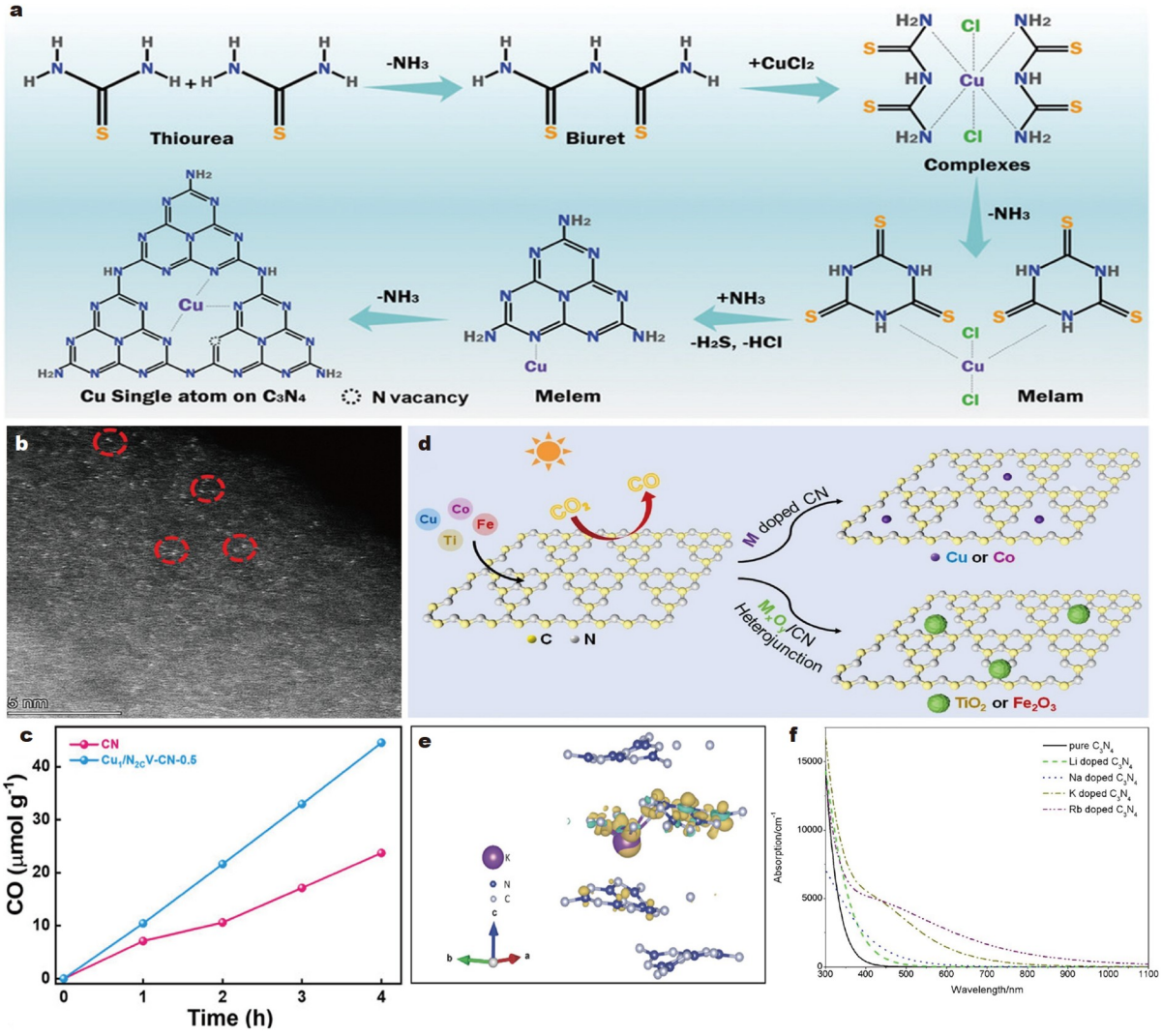

Figure 8 (a) Schematic diagram for the formation mechanism of $Cu_1/N_{2C}V$-CN. (b) Aberration-corrected high-angle-annular-dark-field scanning transmission electron microscopy (AC HAADF-STEM) image of $Cu_1/N_{2C}V$-CN-0.5. (c) Photocatalytic performances of CN and $Cu_1/N_{2C}V$-CN-0.5 samples for CO_2 photocatalytic reduction under light irradiation. Reprinted with permission from Ref. [109]. Copyright 2023, Wiley. (d) Mechanism diagram of transition metals incorporated CN (MeCN, Me = Cu, Co, Ti or Fe). Reprinted with permission from Ref. [110]. Copyright 2022, Elsevier. (e) Charge difference distribution of K-CN. Reprinted with permission from Ref. [106]. Copyright 2020, American Chemical Society. (f) Simulated absorption spectra of g-C_3N_4 doped with different alkali metals. Reprinted with permission from Ref. [108]. Copyright 2020, Elsevier.

pristine g-C_3N_4. Zhang *et al.* [108] prepared alkali metal (Li, Na, K, Rb)-doped g-C_3N_4 using a hydrothermal and high-temperature calcination method. The calculated results showed a significant increase in the absorption spectrum of Rb-doped g-C_3N_4 within the range of 500 to 1100 nm, consistent with the UV–vis spectra (Fig. 8f). Compared with bulk g-C_3N_4, Rb-doped g-C_3N_4 exhibited the best CO_2 photoreduction performance, with a more than threefold increase in CO production. Experimental and theoretical evidence demonstrated that the enrichment of surface electrons and optimization of the electronic structure on the catalyst surface were crucial factors in enhancing the photocatalytic performance.

Nonmetallic doping

Nonmetal element doping can effectively reduce the bandgap of g-C_3N_4, thereby enhancing its light harvesting capability. Unlike metal elements, nonmetal elements play a unique role in enhancing light absorption and modulating the energy band positions for efficient redox reactions [111]. Furthermore, due to their high electronegativity and ionization potential, nonmetal elements can typically form covalent bonds by gaining electrons from other compounds. Several nonmetal elements have been studied for their ability to enhance the CO_2 reduction efficiency in g-C_3N_4, including B [68,112], P [113–115], O [66,116,117], S [18,118,119], Se [120], F [121,122], Cl [123], Br [124,125], I [126], and others.

Arumugam *et al.* [127] prepared nonmetal (B, O, P, and S)-doped g-C_3N_4 through solid-state condensation of urea. The highest CH_4 yield of 55.10 nmol $(mL_{H_2O}\ g_{cat})^{-1}$ was achieved with S-doped g-C_3N_4 after 7 h of irradiation (UV) (Fig. 9a, b). The results demonstrated that nonmetal element doping improved the charge separation and served as an effective pathway to enhance photocatalyst performance. Yan *et al.* [124] prepared surface-brominated g-C_3N_4 (CNBr) for the stable and

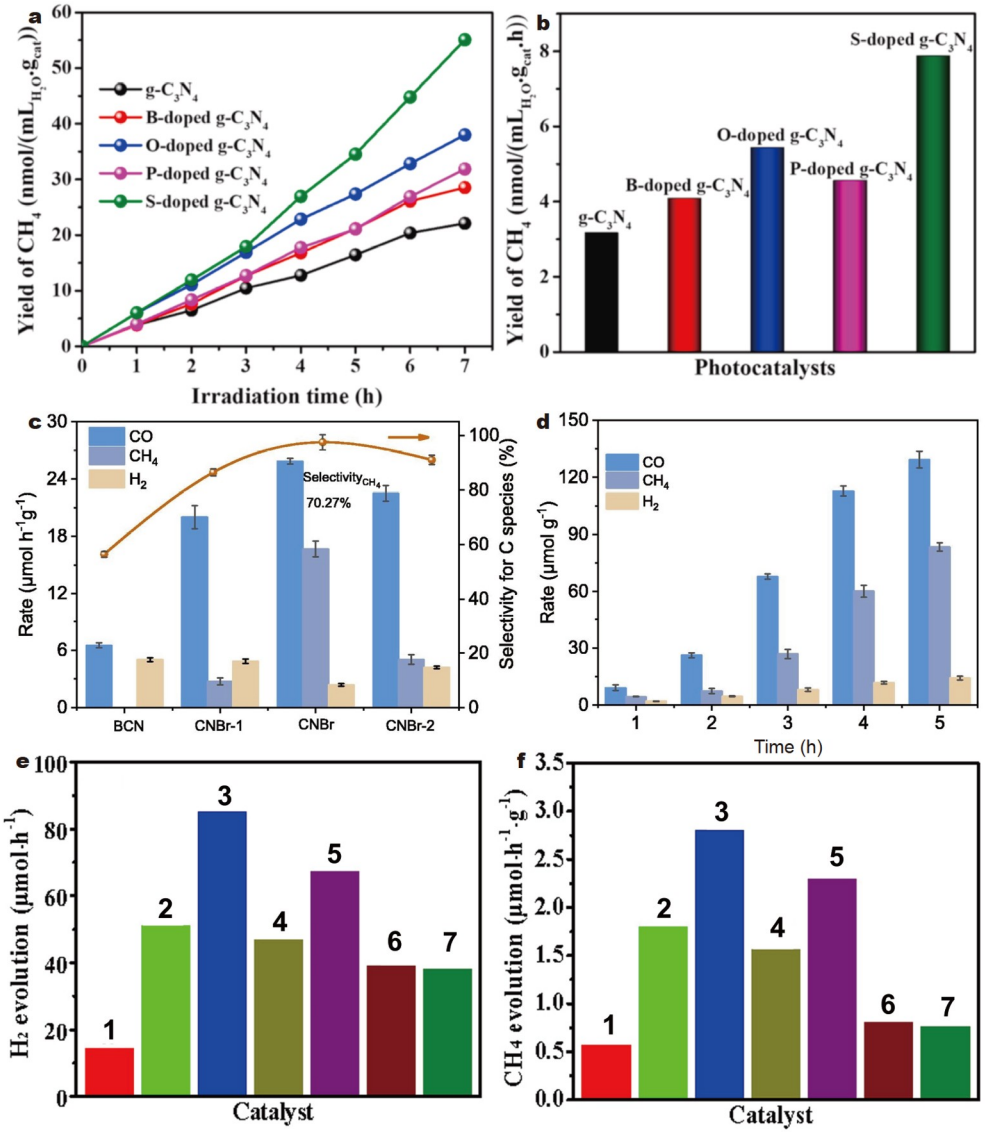

Figure 9 (a) Photocatalytic CO_2 reduction into CH_4 with various irradiation times and (b) the maximum formation rates of CH_4 over bare g-C_3N_4, B, O, P and S doped g-C_3N_4 photocatalysts. Reprinted with permission from Ref. [127]. Copyright 2022, Elsevier. (c) Activities of CNBr and BCN materials for photocatalytic CO_2 reduction. (d) Time-dependent yields of CNBr photocatalytic CO_2 reduction. Reprinted with permission from Ref. [124]. Copyright 2023, Elsevier. (e) Photocatalytic H_2 evolution rates and (f) photocatalytic CH_4 evolution rates for (1) CN, (2) CN/CNI-20%, (3) CN/CNI-40%, (4) CN/CNI-40% (physical mixture), (5) CN/CNI-60%, (6) CNI, and (7) CNI-R catalysts under visible-light irradiation (λ > 420 nm). Reprinted with permission from Ref. [126]. Copyright 2020, Elsevier.

efficient photocatalytic reduction of CO_2 to generate CH_4, achieving a reaction rate of 16.68 μmol h^{-1} g^{-1} (with a selectivity of 70.27%) (Fig. 9c, d). By utilizing Br as an active site, CO_2 could accumulate on the catalyst surface, and localized photo-excited electrons could activate the adsorbed CO_2, leading to subsequent hydrogenation and the generation of CH_4. Xia *et al.* [126] employed a combination of a water bath method and *in situ* sintering to prepare g-C_3N_4/iodine-doped g-C_3N_4 (CN/CNI) homojunction powder catalysts. The CN/CNI-40% catalyst with a proper CN content had good visible light photocatalytic performance and stability. The rates of photocatalytic CH_4 generation were 4.9, 3.5, and 3.6 times greater than those of CN, CNI, and CNI-R, respectively (Fig. 9e, f). Generally, due to their smaller atomic radii, the F and Cl atoms are doped mainly by substituting C or N, while Br and I, with larger atomic radii, are difficult to substitute and are more likely to be doped into the gaps between three tri-*s*-triazine units. Research has shown that the work function of g-C_3N_4 decreases with increasing atomic number of halogen dopants. This occurs because the electronegativity of halogen atoms gradually decreases with increasing atomic number, resulting in more electrons transferring from halogen atoms to g-C_3N_4; thus, the Fermi level of g-C_3N_4 increases and the work function decreases, thereby enhancing its photocatalytic performance [79].

In summary, nonmetal doping adjusts the band structure of g-C_3N_4, resulting in a narrower band gap and an extended light absorption range to the visible region, thereby enhancing its photocatalytic performance in CO_2 reduction. Introducing impurity elements into g-C_3N_4 also facilitates the alteration of the surface charge distribution, promoting the separation and transfer of photoinduced charge carriers. Additionally, the incorporation of nonmetal elements may favour CO_2 adsorption.

Heterojunction engineering

A heterojunction refers to the interface of two different semiconductor materials with different atomic and electronic band structures. Among the existing strategies for regulating g-C_3N_4, interface engineering to construct heterojunctions by coupling g-C_3N_4 to different semiconductors has gained research interest. The construction of heterostructures can facilitate the photoinduced electron and hole separation. Under the action of a heterojunction electric field, electrons can migrate through the semiconductor, thereby improving the charge transfer efficiency and effectively inhibiting the recombination of photogenerated charges and holes. Traditional heterojunctions can be classified into three types based on the relationship between energy bands: straddling gaps (Type-I heterojunctions, Fig. 10a), staggered gaps (Type-II heterojunctions, Fig. 10b) and broken gaps (Type-III, heterojunctions, Fig. 10c). However, among the three heterojunctions, only Type-II heterojunctions can achieve effective interface transfer and spatial separation of the electron-holes under photoexcitation. This occurs because under light conditions, after the generation of electron-hole pairs, electrons can transfer from photonic crystal (PC) I to PC II, and the photogenerated holes move in the opposite direction to achieve the spatial separation of photogenerated electrons and holes. Type-I heterojunctions and type-III heterojunctions can only achieve effective interfacial transfer of electrons and holes under photoexcitation conditions but not spatial separation of electrons and holes. To further improve the catalytic effect of photocatalysts, in which the electrons accumulate at higher energy levels and the holes accumulate at lower energy levels, to enhance the redox ability of photocatalysts, researchers have developed heterojunctions such as Z-scheme heterojunctions and S-scheme heterojunctions. The construction of a suitable heterostructure based on g-C_3N_4 not only solves the problem of low photogenerated carrier separation efficiency in the original g-C_3N_4 but also improves the photocatalytic photoelectric performance in conjunction with other components of the heterostructure. Therefore, constructing heterostructures based on g-C_3N_4 has become a popular for improving the performance of photocatalytic CO_2 reduction. Currently, the main semiconductors consisting of heterostructures with g-C_3N_4 include metal oxides (TiO_2, ZnO, NiO, CeO_2, etc.), metal sulfides (SnS_2, $CdIn_2S_4$, Bi_2S_3, etc.), and other nonmetallic semiconductors [128]. According to the different mechanisms of the photoinduced carrier transfer between g-C_3N_4 and the coupled component, the most studied g-C_3N_4-based heterostructure photocatalysts can be divided into the following types: g-C_3N_4-based type-II heterostructures, g-C_3N_4-based Z-scheme heterostructures, g-C_3N_4-based S-scheme heterostructures and other types of g-C_3N_4-based heterojunctions.

g-C_3N_4-based type-II heterostructures

Type II heterojunction nanocomposites possess staggered bandgaps and appropriate CB and VB. When the CB of PC I is more negative than that of PC II and the VB of PC II is more positive than that of PC I, under the driving force of the built-in electric field, the electrons in the CB of PC I transfer to the CB of PC II, and the holes in the VB of PC II transfer to the VB of PC I. CO_2 is reduced to hydrocarbon compounds on the CB of PC II. The effective charge transfer at the interface of the two semiconductors achieves efficient separation of photoinduced carriers, thereby preventing the recombination of photoinduced electrons and holes (Fig. 10b).

Xu *et al.* [129] first used a molten salt growth method to prepare exposed Bi_4NbO_8Cl nanosheets and then fabricated 2D/2D Bi_4NbO_8Cl/g-C_3N_4 heterostructure photocatalysts through high-energy ball milling and subsequent sintering, achieving a closely interacting interface (Fig. 11a, b). All Bi_4NbO_8Cl/g-C_3N_4 composite materials exhibited significantly improved photocatalytic activity compared with Bi_4NbO_8Cl nanosheets and g-C_3N_4, showing enhanced CO production activity for photocatalytic CO_2 reduction, with a yield of 2.26 μmol g^{-1} h^{-1}. The remarkable increase in the photocatalytic activity of the Bi_4NbO_8Cl/g-C_3N_4 composite materials was attributed to the synergistic effect of the well-defined 2D/2D structure, the con-

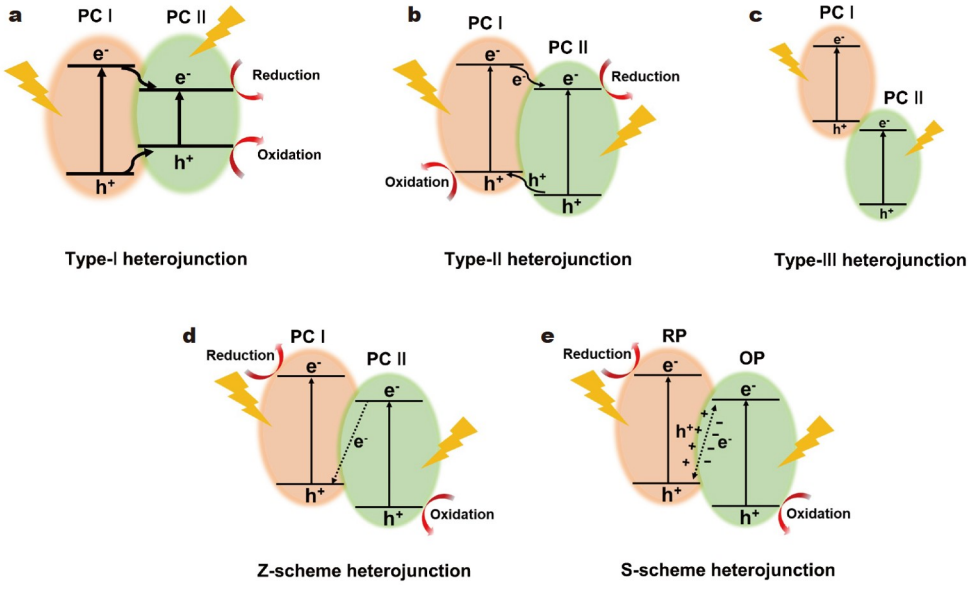

Figure 10 Schematic diagram of three common g-C_3N_4 base heterojunctions. (a) g-C_3N_4-based Type-I heterostructure. (b) g-C_3N_4-based Type-II heterostructure. (c) g-C_3N_4-based Type-III heterostructure. (d) g-C_3N_4-based Z-scheme heterostructure. (e) g-C_3N_4-based S-scheme heterostructure.

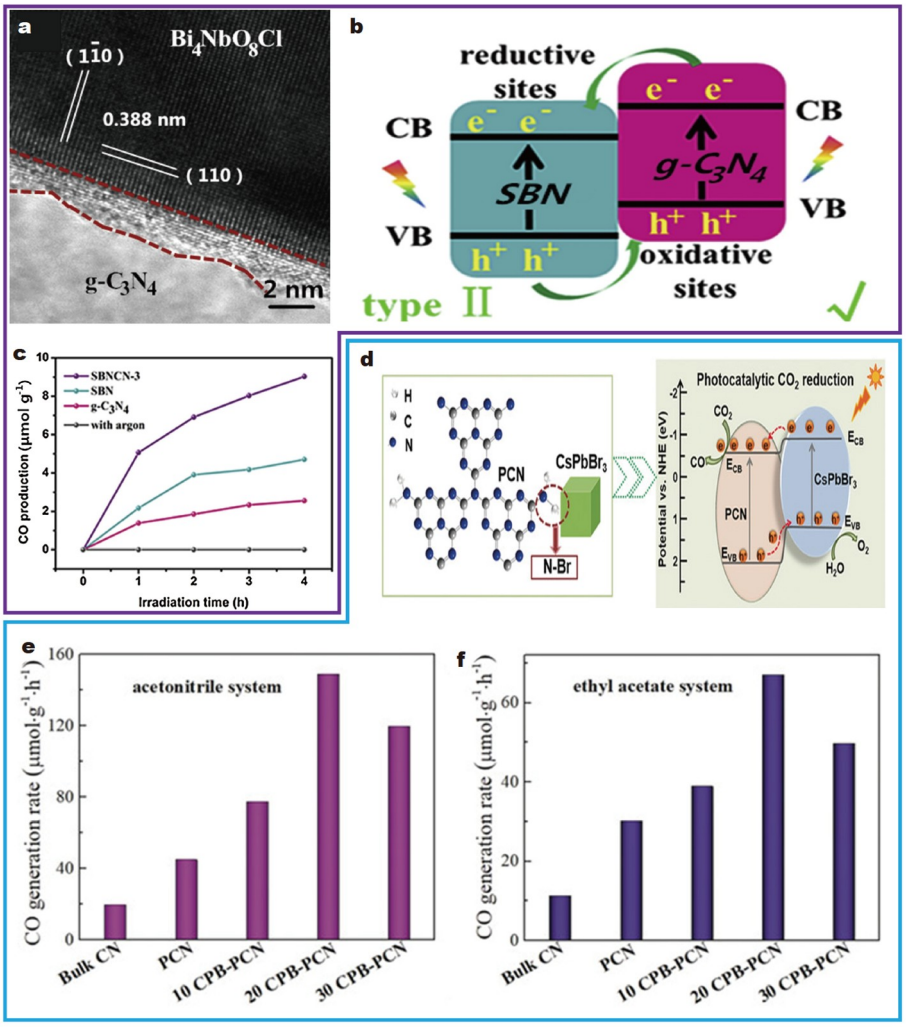

Figure 11 (a) High-resolution TEM (HRTEM) image of $Bi_4NbO_8Cl/g\text{-}C_3N_4$ composite (SBNCN-3). (b) Photocatalytic mechanism of type-II heterojunction between Bi_4NbO_8Cl and $g\text{-}C_3N_4$. (c) CO production curves of SBNCN-3, SBN and $g\text{-}C_3N_4$. Reprinted with permission from Ref. [129]. Copyright 2020, Elsevier. (d) $CsPbBr_3$ quantum dots are fixed on polymer semiconductor $g\text{-}C_3N_4$ porous nanosheets by strong N–Br bond to form type-II heterojunction. Generation of CO in (e) acetonitrile/water and (f) ethyl acetate/water systems over various photocatalysts. Reprinted with permission from Ref. [130]. Copyright 2018, Wiely.

struction of type II heterojunctions, and the close interaction interface, which promoted the charge separation (Fig. 11c). Ou *et al.* [130] anchored $CsPbBr_3$ quantum dots (CPBs) onto porous $g\text{-}C_3N_4$ nanosheets (PCNs) rich in $-NH_x$ to construct a type-II heterojunction through N–Br chemical bonding (Fig. 11d). The unique N–Br bonding enhanced the charge separation between the two materials and prolonged the lifetime of the carriers. The CPB-PCN photocatalyst with 20 wt% quantum dots exhibited excellent stability and achieved a CO production rate of 149 μmol h^{-1} g^{-1} for photocatalytic CO_2 reduction in acetonitrile/water under visible light irradiation, which was approximately 15 times greater than that of $CsPbBr_3$ quantum dots (Fig. 11e, f).

Wang *et al.* [131] prepared titanium dioxide (TiO_2)-modified $g\text{-}C_3N_4$ composite photocatalysts through ball milling and calcination. The study showed that TiO_2 successfully formed a type-II heterojunction with $g\text{-}C_3N_4$, effectively improving the separation of photoinduced electrons and holes. Compared with the pure $g\text{-}C_3N_4$ photocatalysts, the heterojunction photocatalysts exhibited significantly enhanced photocatalytic CO_2 reduction. Under 8 W UV light irradiation for 4 h, the production rates of CH_4 and CO were 72.2 and 56.2 μmol g^{-1}, respectively. Li *et al.* [132] designed and synthesized mesoporous CeO_2/graphitic carbon ($m\text{-}CeO_2/g\text{-}C_3N_4$) type-II heterostructures using a hard template method. Their study demonstrated that the photocatalytic response of $m\text{-}CeO_2/g\text{-}C_3N_4$ was significantly enhanced, enabling the efficient separation and transfer of photoinduced carriers at the interface of mesoporous CeO_2 and $g\text{-}C_3N_4$. Therefore, $m\text{-}CeO_2/g\text{-}C_3N_4$ markedly enhanced the photocatalytic reduction of CO_2. After 1 h of CO_2 reduction using a 50 mg nanocomposite photocatalyst, the production rates of CO and CH_4 were 0.590 and 0.694 μmol, respectively.

Based on these studies, the formation of type-II heterostructures between semiconductors with suitable band structures and $g\text{-}C_3N_4$ can effectively suppress the rapid recombination of photoinduced electron-hole pairs and promote the separation and transfer of photoinduced carriers to the catalyst surface for CO_2 reduction. However, efficient charge separation in type-II heterostructures is achieved at the expense of sacrificing pho-

toinduced carriers with strong redox capability, which limits the thermodynamic requirements of photocatalytic CO_2 reduction [133].

g-C_3N_4-based Z-scheme heterojunctions

Due to the increased coulombic repulsion between the electrons during the process of electron transfer from the CB of one semiconductor to the VB of another semiconductor, the application of type II photocatalysts is limited. Additionally, after electrons are transferred to a semiconductor with a lower potential, the photocatalytic reduction capability is relatively low, providing an opportunity for the research and development of Z-scheme heterostructures. In Z-scheme heterostructures, electrons in the CB of PC II can undergo interface transfer and recombine with the VB of PC I, and this process enables the participation of carriers from both CB of PC I and VB of PC II in the redox process and is unaffected by electron-hole recombination (Fig. 10d). Z-scheme heterostructures involve the close alignment of the Fermi energy levels of two semiconductors, resulting in inwards band bending at their band edges. This facilitates the movement of electrons from the CB of the oxidizing semiconductor to the VB of the reducing semiconductor, contributing to improved redox potentials and enhanced photocatalytic activity. Furthermore, due to the sufficiently negative CB position of g-C_3N_4, which exhibits strong reduction ability, g-C_3N_4 tends to form Z-scheme heterostructures with photocatalysts possessing a sufficiently positive VB potential, thereby attaining enhanced oxidation capability [134].

Jiang *et al.* [134] employed a hierarchical direct Z-scheme system composed of sea urchin-like haematite and g-C_3N_4 to enhance the photocatalytic activity for CO_2 reduction. They achieved a CO production rate of 27.2 μmol g^{-1} h^{-1} without the need for auxiliary catalysts or sacrificial agents; additionally, this rate was 2.2 times higher than that using g-C_3N_4 alone (10.3 μmol g^{-1} h^{-1}). The introduction of 3D α-Fe_2O_3 increased light absorption capacity (due to its narrow bandgap), enabling more light energy to participate in CO_2 reduction. Wang *et al.* [135] synthesized a novel MnO_2/g-C_3N_4 Z-scheme heterostructure composite material for the first time by *in situ* redox reaction of $KMnO_4$ with adsorbed $MnSO_4{\cdot}H_2O$ on the surface of g-C_3N_4. The formation of the Z-scheme heterostructure enhanced the photocatalyst's light absorption capacity, and the well-matched band structures facilitated effective separation of photoinduced electrons and holes, thereby enhancing the photocatalytic activity for CO_2 reduction. Bhosale *et al.* [136] prepared a g-C_3N_4/$FeWO_4$ Z-scheme heterostructure composite material capable of selectively reducing CO_2 to CO as a solar fuel under sunlight. The Z-scheme coupling of visible light-active $FeWO_4$ nanoparticles and g-C_3N_4 nanosheets demonstrated excellent CO production rates, reaching 6 μmol g^{-1} h^{-1} at room temperature; this value was nearly six times higher than that of pristine g-C_3N_4 and fifteen times higher than that of pristine $FeWO_4$. Furthermore, the selectivity for CO was 100% higher than other carbon products from CO_2 reduction and more than 90% higher than hydrogen products from water splitting.

In summary, Z-scheme heterostructures composed of two different semiconductor materials can optimize the band structure by adjusting the bandgap sizes and energy level structures of different materials. This enables high efficiency in the separation of electrons and holes, effectively converting light energy into chemical energy for CO_2 reduction and enhancing photocatalytic activity. Z-scheme heterostructures achieve selective control over different reaction products by matching and adjusting the band positions, leading to highly selective CO_2 reduction. Moreover, the fabrication process of Z-scheme heterostructures is relatively simple, enabling the synthesis of different forms and structures through various methods; thus, superior photocatalytic performance and reaction outcomes with good scalability are attained.

g-C_3N_4-based S-scheme heterojunctions

The charge transfer process in S-scheme heterojunctions is illustrated in Fig. 10e. This type of heterojunction is primarily composed of a reducing semiconductor photocatalyst (RP) with a smaller work function and higher Fermi level and an oxidizing semiconductor photocatalyst (OP) with a larger work function and lower Fermi level. The S-scheme heterojunction facilitates the efficient spatial separation of the electron-hole pairs with strong redox capabilities. In the S-scheme heterojunction, the combination of the built-in electric field, band bending, and electrostatic interaction enables the spatial separation of photogenerated electrons and holes in a strong redox environment [137]. Under the driving force of the built-in electric field and band bending, the accumulated holes on the VB of OP are consumed by sacrificial agents, and the accumulated electrons on the CB of RP react with CO_2 to produce other products. Therefore, constructing S-scheme heterojunctions based on g-C_3N_4 significantly enhances the photocatalytic performance of CO_2 reduction. Generally, g-C_3N_4 is a typical RP and tends to form S-scheme heterojunctions with OPs such as TiO_2, $BiVO_4$, WO_3, Ag_3PO_4, CeO_2, ZnO, and $SrTiO_3$ [138].

He *et al.* [139] synthesized a TiO_2/g-C_3N_4 composite material with surface-loaded Ti_3C_2 MXene quantum dots (TCQD) for the efficient photocatalytic reduction of CO_2 into hydrocarbon fuels (Fig. 12a). The presence of TCQDs accelerated the spatial migration of electrons on the CB of g-C_3N_4, serving as a channel and acceptor for electron transfer. The results demonstrated that the synergistic effect of the S-scheme heterojunction and TCQDs significantly enhanced the photocatalytic reduction activity of CO_2, with a CO evolution rate of 4.39 μmol g^{-1} h^{-1}; this value was three times higher than that of individual C_3N_4 and TiO_2 (Fig. 12b). Xie *et al.* [140] successfully constructed a bifunctional ternary g-C_3N_4/Bi/$BiVO_4$ hybrid photocatalyst, which exhibited excellent aerobic photocatalytic oxidation performance for organic pollutant degradation and impressive photocatalytic CO_2 reduction performance under anaerobic conditions. The exceptional dual-functional photocatalytic performance of the g-C_3N_4/Bi/$BiVO_4$ hybrid photocatalyst was attributed to the formation of efficient S-scheme hybrid junctions, which not only greatly promoted appropriate charge dynamics but also maintained good charge potentials. Moreover, the introduction of metallic Bi nanoparticles enhanced visible light absorption through the surface plasmon resonance (SPR) effect and promoted interfacial charge transfer through the S-scheme bridging effect (Fig. 12c). Zhou *et al.* [141] constructed a new lead-free double perovskite Cs_2TeBr_6 that combined with metal-free semiconductor g-C_3N_4 to form S-scheme heterojunction, and this heterojunction was first used for photocatalytic CO_2 reduction (Fig. 12d). The formation of S-scheme heterojunctions led to efficient space charge separation and preserved the strong electrons and holes, thus enhancing photocatalytic activity. The results showed that the 5%-CTB/CN heterojunction material

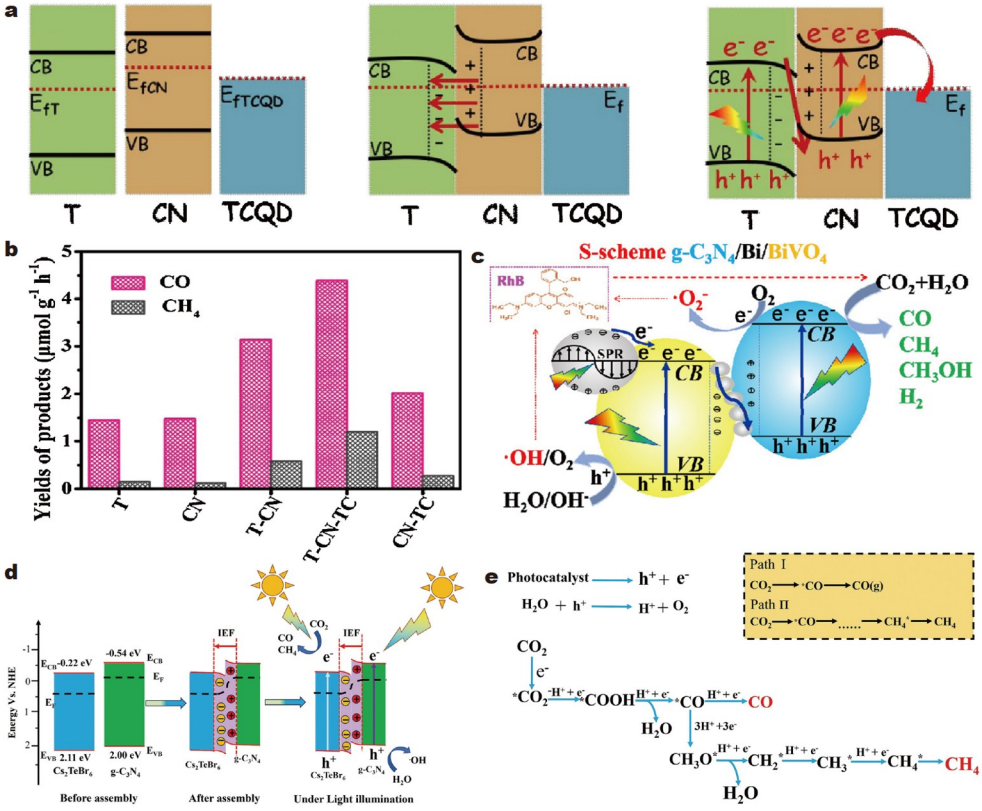

Figure 12 (a) S-scheme heterojunction of $TiO_2/C_3N_4/Ti_3C_2$ quantum dots: before contact, after contact, and after contact upon irradiation and charge migration and separation. (b) Photocatalytic CO_2 reduction performance of the prepared samples after irradiation for 1 h. Reprinted with permission from Ref. [139]. Copyright 2020, Elsevier. (c) Bifunctional S-scheme g-C_3N_4/Bi/$BiVO_4$ hybrid photocatalysts demonstrate both superior aerobic photocatalytic organic pollutant oxidation performance and impressive anaerobic photocatalytic CO_2 reduction ability. Reprinted with permission from Ref. [140]. Copyright 2020, Elsevier. (d) Diagram of S-scheme charge transfer process in CTB/CN heterojunction. (e) Schematic diagram of reaction routes for CO_2 photoreduction. Reprinted with permission from Ref. [141]. Copyright 2023, Wiley.

exhibited the best photocatalytic reduction of CO_2 under visible light irradiation. After 3 h of light exposure, the yields of CO and CH_4 were 468.90 and 61.31 μmol g^{-1}, respectively. The yield of CO was 1.5 and 32 times higher than those of pure Cs_2TeBr_6 and g-C_3N_4, and the yield of CH_4 was 2 times higher than that of pure Cs_2TeBr_6. Furthermore, based on the *in situ* Fourier transform infrared (FT-IR) test results, the reaction route of CO_2 photoreduction was proposed (Fig. 12e).

The bandgap of the S-scheme heterojunction could match the visible and even UV regions, providing the heterojunction with high catalytic activity in the photocatalytic CO_2 reduction reaction and significantly improving the reaction rates and product selectivity. The excellent charge transfer performance of the S-scheme heterojunction can effectively promote the separation and transfer of photoinduced charge carriers, thereby improving the photoelectrochemical conversion efficiency and enhancing the catalytic performance of photocatalytic CO_2 reduction.

g-C_3N_4-based heterojunctions of other types

In addition to the aforementioned heterojunction types, other g-C_3N_4-based heterojunctions for CO_2 reduction mainly include multivariate heterojunctions and Schottky heterojunctions. They have also been shown to have excellent photocatalytic CO_2 reduction properties.

The unique geometry and photocatalytic system composition of ternary heterojunction catalysts have many advantages, such as short diffusion length and high conductivity for efficient charge separation and transport and high specific surface area and effective active site for enhanced photoredox catalytic activity. Saikia's group [142] used a ternary heterojunction photocatalyst consisting of g-$C_3N_4/Ni_{12}P_5/ZnIn_2S_4$ to convert CO_2 to methanol. When the ratio of $ZnIn_2S_4$ to NPCN was 0.1, the heterojunction could provide the maximum methanol yield of 164 μmol g^{-1}; this value was 1.5 and 3.1 times higher than those of binary $Ni_{12}P_5$/g-C_3N_4 (NPCN) and $ZnIn_2S_4$/g-C_3N_4 (CNZ), respectively. The optimized model (Fig. 13a) showed that the doping of $Ni_{12}P_5$ and $ZnIn_2S_4$ led to a certain distortion of g-C_3N_4, and the calculated adhesion energy of −1.3 eV confirmed the stability of the heterojunction structure. As indicated by the surface projected density of states (PDOS) (Fig. 13b), in the ternary NCZ heterojunction, the valence band maximum (VBM) was contributed by $Ni_{12}P_5$, while the conduction band maximum (CBM) was mainly composed of $ZnIn_2S_4$, which could provide stability to the heterojunction. Furthermore, the reduced band gap in the ternary heterojunction produced a more effective photocatalyst than the binary composite. This study elucidated the important role of transition metal phosphides as an electronic bridge between two components forming a ternary heterojunction to improve photocarrier separation efficiency and provided a new perspective for the design of highly reactive photoactive materials for CO_2 photoreduction. In

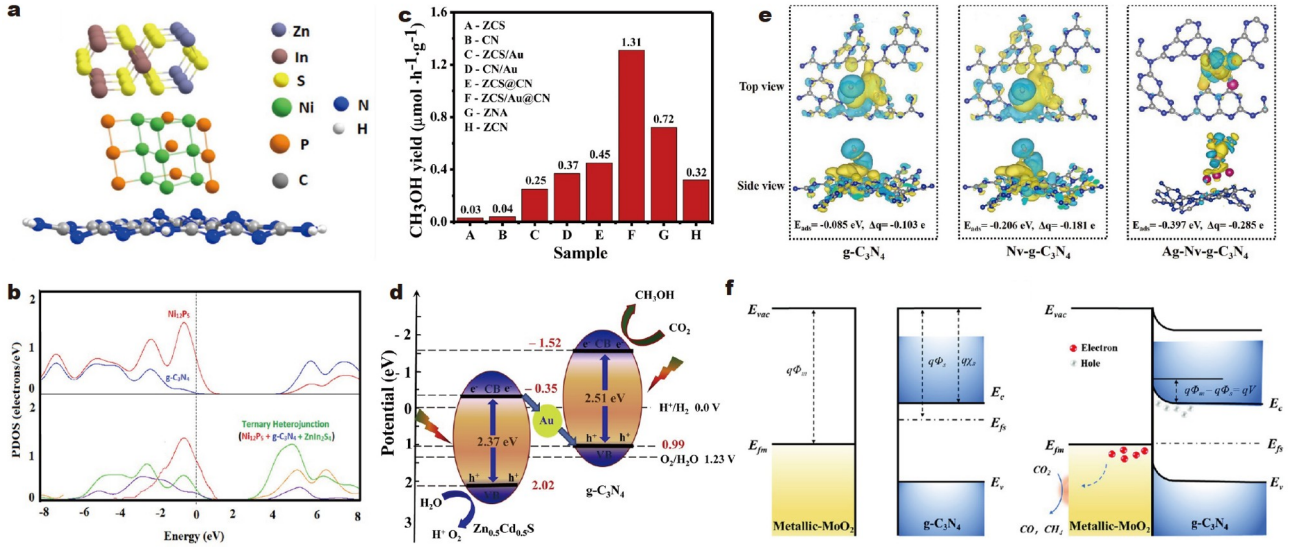

Figure 13 (a) Optimised structural model of g-C_3N_4-$Ni_{12}P_5$-$ZnIn_2S_4$. (b) PDOSs of $Ni_{12}P_5$ and g-C_3N_4 surfaces and ternary g-C_3N_4-$Ni_{12}P_5$-$ZnIn_2S_4$ heterojunction surface. Reprinted with permission from Ref. [142]. Copyright 2023, American Chemical Society. (c) Comparison of the rate of generation of CH_3OH from ZCS/Au@CN with other materials. (d) Schematic Z-scheme mechanism of charge-transfer processes for photocatalytic CO_2 reduction over ZCS/Au@CN heterojunction under visible light irradiation. Reprinted with permission from Ref. [143]. Copyright 2021, Elsevier. (e) Differential charge densities of the adsorbed CO_2 molecule on g-C_3N_4, Nv-g-C_3N_4, Ag-Nv-g-C_3N_4. Reprinted with permission from Ref. [144]. Copyright 2022, Elsevier. (f) Schematic representation of the Fermi levels and band structures before and after contact between MoO_2 and g-C_3N_4. Reprinted with permission from Ref. [145]. Copyright 2020, Wiley.

addition, Cheng's group [143] used a simple photodeposition hydrothermal method to prepare $Zn_xCd_{1-x}S$/Au@g-C_3N_4 heterojunction composite photocatalyst, and good contact was achieved among ZCS, AuNPs, and CN. The catalyst showed a high CH_3OH formation rate (1.31 μmol h^{-1} g^{-1}), which was approximately 43.6 and 32.7 times higher than those of the pure ZCS and CN samples, respectively (Fig. 13c). As shown in Fig. 13d, a mechanism for the enhanced CO_2 reduction performance was proposed and included the formation of Fermi level equilibrium at the ZCS, Au, and CN interfaces before illumination and the rapid migration of electrons on ZCS CB to AuNPs after illumination. Thus, the electrons accumulated in the high potential CB of CN could reduce CO_2 to CH_3OH, while the holes left in the VB of ZCS promoted the photooxidation process to generate H^+ and reactive oxygen species. The results from this study showed that the development and application of ternary heterojunctions facilitated the further development of the photocatalytic reduction of CO_2, and this research strategy could also be extended to other solar-related applications.

The g-C_3N_4 can also form Schottky heterojunctions with metal nanoparticles to enhance carrier migration. g-C_3N_4-based Schottky heterojunctions with metals can provide effective catalytically active centres to further enhance the photocatalytic performance of g-C_3N_4. Plasmonic Ag NPs were successfully constructed by *in situ* self-assembly on nitrogen vacancy-modified g-C_3N_4 nanotubes (ACNNTs); this process produced highly efficient visible-light photocatalytic CO_2 conversion (88.2 μmol g^{-1} h^{-1}), which was more than 10.9 times that of BCN[144]. As shown in Fig. 13e, the DFT calculations indicated that the introduction of nitrogen vacancies could change the Schottky potential barrier at the interface while lowering the energy barrier for CO_2 activation. Therefore, the optimized Schottky barrier height not only accelerated the charge dynamics through the driving force of the Schottky junction but also prevented the photoelectrons captured by Ag from flowing back to g-C_3N_4 in the visible light; this effectively inhibited photogenerated carrier complexation, leading to a more efficient CO_2 photoreduction. This study revealed the significance of carbon nitride-based Schottky heterojunctions in the field of photocatalytic CO_2 reduction. In addition to metal nanoparticles, the formation of Schottky heterojunctions with metal oxides and g-C_3N_4 could solve the problems of low carrier separation rate and low surface activity of g-C_3N_4. Qiu's group [145] constructed Schottky heterojunctions by loading and optimizing MoO_2 with metallic properties on g-C_3N_4 to improve the photocatalytic CO_2 reduction activity. As shown in Fig. 13f, due to the built-in electric field, MoO_2 was able to rapidly abstract photogenerated electron-hole pairs, accelerate the separation of photogenerated electron-hole pairs, and enhance the CO_2 activity of g-C_3N_4. This study provided a new concept in improving the CO_2 reduction performance of g-C_3N_4 photocatalytic materials.

Noble metal deposition

Noble metal deposition can enhance the number of catalytic active sites and the surface area of photocatalytic materials, adjust the surface electronic structure of the photocatalytic material, promote charge transfer, and suppress photocorrosion. Deposition of noble metals can introduce localized SPR effects, enhancing light absorption capacity and improving the efficiency of photocatalytic reactions. Additionally, the localized surface electric field of noble metals can accelerate the separation and transfer of photoinduced charge carriers, thereby enhancing the effectiveness of photocatalytic CO_2 reduction reactions. Using noble metals as catalysts can significantly improve the photocatalytic performance of g-C_3N_4 semiconductors and the selectivity of CO_2 reduction products. Noble metal nanoparticles can effectively activate CO_2 adsorbed on the surface of g-C_3N_4 since they have higher work functions and lower Fermi levels

when deposited on the surface. The combination of noble metals with semiconductors forms composite materials, leading to an upwards bending of the energy band of g-C_3N_4 and improving the charge separation efficiency [146]. Due to its bending, the total Fermi level of the composite material shifts to a more negative potential, and the bending ultimately balances with the Fermi level of the semiconductor. Noble metals become reservoirs for photoinduced electrons on the semiconductor surface, forming Schottky junctions that prevent electrons from flowing back into the semiconductor. Consequently, electron accumulation occurs in the metal, while hole accumulation occurs in the semiconductor, thereby enhancing photocatalytic performance [147]. Currently, the noble metals used for modifying g-C_3N_4 catalytic activity mainly include Pt [148,149], Au [150,151], Ag [152,153], Pd [154,155], and others. The deposition of these noble metals can significantly improve the catalytic efficiency of g-C_3N_4 in photocatalytic CO_2 reduction.

Yu *et al.* [148] deposited a certain amount of Pt on the surface of g-C_3N_4 to prepare g-C_3N_4-Pt nanocomposites (Fig. 14a). With an increase in Pt content from 0 to 0.75 wt%, the yields of CH_3OH and HCHO also increased and reached their maximum value at a Pt content of 0.75 wt% (Fig. 14b). Their study demonstrated that Pt nanoparticles could effectively promote the transfer and enrichment of photoinduced electrons from g-C_3N_4 to its surface, thereby enhancing the photocatalytic CO_2 reduction capability of g-C_3N_4-Pt nanocomposites. Li *et al.* [150] employed a method involving $HAuCl_4{\cdot}3H_2O$ impregnation of g-C_3N_4 powder and N_2 plasma treatment to prepare gold nanoparticle (CN/Au)-modified amino-functionalized g-C_3N_4. CN/Au exhibited strong photocatalytic activity for CO_2 reduction under visible light irradiation without the addition of auxiliary catalysts or sacrificial agents (Fig. 14c). The CO and CH_4 evolution rates for CN/Au were 28.3 and 1.3 μmol h^{-1} g^{-1}, respectively, which were 7.6 and 2.6 times higher than those of pristine g-C_3N_4 (CN-0) (Fig. 14d). Cao *et al.* [154] showed the significant effects of Pd cocatalysts on CO_2 photoreduction on g-C_3N_4. By adjusting the quantities of (1 1 1) and (1 0 0) facets, the surface atomic structure of Pd cocatalysts could be precisely controlled, thereby regulating the interface charge carrier transfer, CO_2 adsorption, and CH_3OH desorption. Their results showed that tetrahedral Pd nanocrystals on the exposed (1 1 1) facets were more favourable for enhancing the photocatalytic performance of g-C_3N_4 in CO_2 reduction compared with cubic Pd nanocrystals on the exposed (1 0 0) facets (Fig. 15a, b). Notably, the CH_3OH production rate for T-CN (3.17 μmol h^{-1} g^{-1}) was 1.42 times higher than that of the C-CN hybrid photocatalyst. Lang *et al.* [155] demonstrated that defect-engineered Pd catalysts greatly enhanced the photocatalytic performance of CO_2 reduction. Their results indicated that the twin-boundary (TB) sites on the surface of Pd cocatalysts were highly active for CO_2 reduction. Based on the proposed mechanism, the photocatalytic activity and selectivity of CO_2 reduction were further enhanced by increasing the surface density of the TB sites and reducing the size of the Pd nanopolyhedra cocatalysts (Fig. 15c, d). Heng *et al.* [152] synthesized mesoporous g-C_3N_4 (MCN) with a high specific surface area and investigated the relationship between CO_2 adsorption capacity and photocatalytic CO_2 reduction activity. Additionally, Ag particles served as active sites, effectively enhancing charge separation efficiency and promoting photocatalytic activity (Fig. 16a). Importantly, the synergistic effect between the mesoporous structure (providing strong CO_2 adsorption capacity) and Ag particles (facilitating efficient charge separation) significantly improved the photocatalytic activity. The CO evolution rate of 3.0% Ag/mesoporous g-C_3N_4

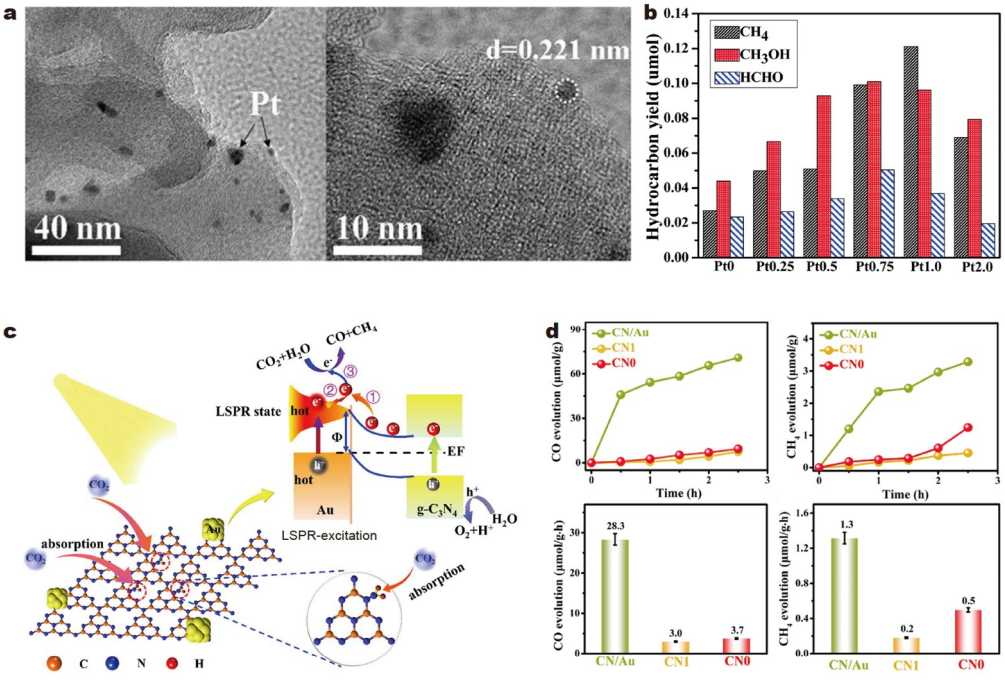

Figure 14 (a) TEM and HRTEM images of the Pt1.0 sample. (b) Comparison of the photocatalytic CH_4, CH_3OH and HCHO-production rates of the Pt0, Pt0.25, Pt0.5, Pt0.75, Pt1.0 and Pt2.0 samples under simulated solar irradiation for 4 h. Reprinted with permission from Ref. [148]. Copyright 2014, Royal Society of Chemistry. (c) Amine-functionalized graphitic carbon nitride decorated with small-sized Au nanoparticles exhibited enhanced photocatalytic activity for CO_2 reduction under visible-light irradiation. (d) Time evolutions of CO and CH_4 over CN/Au, CN1, and CN0. Rates of CO and CH_4 productions by the reduction of CO_2 over CN/Au, CN1, and CN0 under 300 W Xe lamp irradiation. Reprinted with permission from Ref. [150]. Copyright 2020, Elsevier.

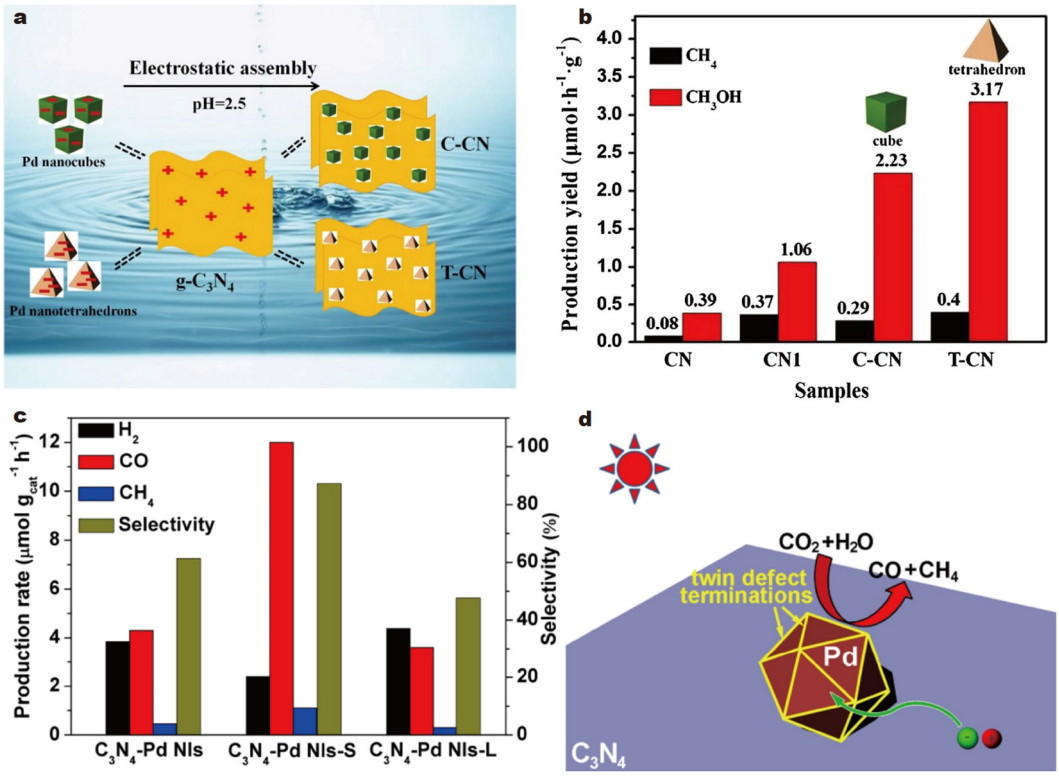

Figure 15 (a) Schematic illustration of the process used for the synthesis of Pd/g-C_3N_4 hybrids. (b) CH_4 and CH_3OH productions over CN, CN1, C-CN and T-CN samples. Reprinted with permission from Ref. [154]. Copyright 2017, Elsevier. (c) H_2, CO, and CH_4 average evolution rates of C_3N_4-Pd NIs-L and C_3N_4-Pd NIs-S in the photocatalytic CO_2 reduction reaction as well as their selectivities for CO_2 reduction with C_3N_4-Pd NIs as a reference sample. (d) Schematic illustrating the proposed mechanism in the photocatalytic CO_2 reduction reaction with C_3N_4-Pd NIs as the catalyst. Reprinted with permission from Ref. [155]. Copyright 2017, IOP Publishing.

(Ag/MCN) reached 1.66 μmol g^{-1} h^{-1}, which was 2.81, 2.41, and 4.37 times higher than that of pristine MCN, 1.0% Ag/bulk g-C_3N_4 (Ag/BCN), and pristine bulk g-C_3N_4 (BCN), respectively (Fig. 16b–e). In addition to single noble metal deposition, the synergistic enhancement of CO_2 photocatalytic activity by multi-noble metal deposition has great research potential. Currently, research on multi-noble metal deposition is relatively scarce. For example, Wang *et al.* [156] demonstrated that Pt-Ag bimetallic nanoparticles deposited on g-C_3N_4 effectively regulated the selectivity and increased the yield of CO_2 reduction products, highlighting the effectiveness of bimetallic structures in enhancing the photocatalytic efficiency of g-C_3N_4 for CO_2 reduction. This research direction may serve as an effective strategy for enhancing the photocatalytic activity of CO_2 reduction.

Other surface modulation methods

In addition to the aforementioned g-C_3N_4 modulation methods, which can effectively enhance the photocatalytic activity of g-C_3N_4 for CO_2 reduction, other modulation strategies can also enhance the photocatalytic activity of g-C_3N_4; these strategies include morphology adjustment, defect engineering, and surface functional group modification. Different morphologies have different specific surface areas and void ratios, and by adjusting the morphology of g-C_3N_4 to increase its specific surface area, more reactive sites can be exposed, thus enhancing the adsorption and reduction reaction of CO_2. In addition, different morphologies of g-C_3N_4 also affect its light absorption properties and thus the CO_2 reduction efficiency. For g-C_3N_4, a variety of different morphologies have been investigated and include 1D rods, tubes, 2D nanosheets, 3D hollow spheres, honeycomb structures, anti-opal structures, and many others [147]. Tian *et al.* [157] prepared porous tubular yolk-shell g-C_3N_4 (PTYS CN-2) by precursor recrystallization (Fig. 17a). The tubular structure increased the light scattering and thus enhanced the light absorption. Due to the enhanced light absorption and abundant reaction sites, the CO yield of PTYS CN-2 was 40.3 μmol g^{-1} at 4 h; this value was 5.6 times higher than that of g-C_3N_4 (Fig. 17b). Ultrathin porous g-C_3N_4 has excellent photocatalytic CO_2 reduction performance. Yang *et al.* [158] prepared ultrathin porous g-C_3N_4 (THCN) with high specific surface area and high CB position using a stepwise synergistic exfoliation method. Their results showed that THCN had the highest efficiency of CO_2 conversion to CH_4 and CO fuel compared with g-C_3N_4 (HCN) prepared by hydrochloric acid-assisted hydrothermal vapour extraction and g-C_3N_4 (TCN) prepared by aerothermal vapour extraction/etching (Fig. 17c, d). Moreover, the excellent photocatalytic CO_2 reduction performance is mainly attributed to its high specific surface area and abundant pores, the good separation and utilization efficiency of the photogenerated carriers, and the more negative position of the CB. Designing defect engineering in the perfect g-C_3N_4 structure to enhance light absorption and drive electron transfer may have a positive effect on CO_2 photocatalytic reduction. Li *et al.* [159] introduced nanodiamond (ND) and nitrogen defects (ND/g-C_3N_4(NH)) on

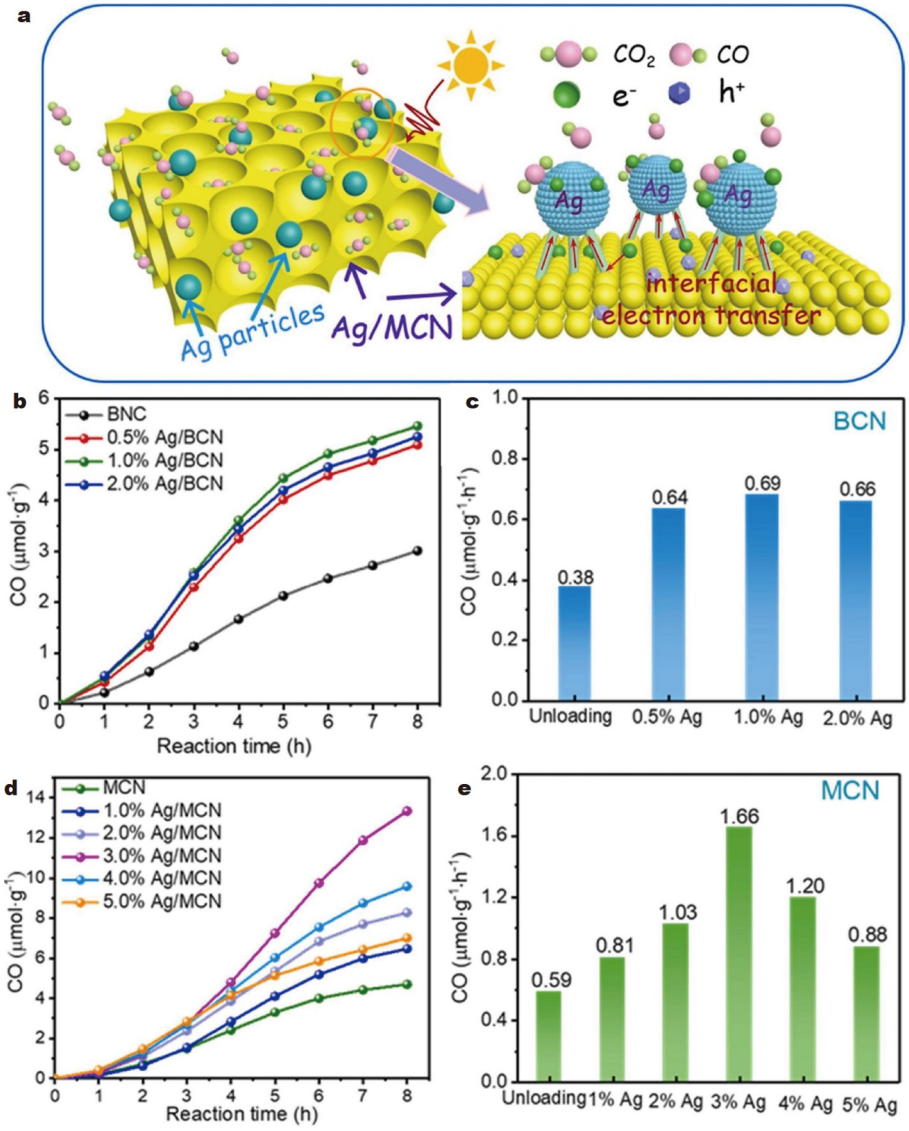

Figure 16 (a) Schematic diagram of the mechanism of enhancing CO_2 photoreduction activity by promoting charge separation and CO_2 adsorption with Ag mesoporous g-C_3N_4. CO evolution rates of Ag/BCN (b, c) and Ag/MCN (d, e) with different loading amounts. Reprinted with permission from Ref. [152]. Copyright 2022, Elsevier.

the g-C_3N_4 surface using an *in situ* thermal polymerization method (Fig. 17e). Under visible light irradiation, ND/g-C_3N_4 (NH) exhibited excellent CO_2 photocatalytic performance with a CO yield of 10.98 μmol h^{-1} (18.6 times higher than that of pristine g-C_3N_4) (Fig. 17f). The synergistic effect of nitrogen vacancy engineering and ND modification improved CO_2 photoreduction, significantly enhanced visible light absorption, promoted electron transfer pathway, and effectively facilitated carrier separation and transfer. Functional group modifications are generally used to change the energy band structure of g-C_3N_4 and the adsorption of CO_2, and some common functional groups, such as carboxylation (carboxylation), amination, sulfonation, hydroxylation, and cyanation, have been used to modify g-C_3N_4 to enhance its photocatalytic activity [146]. Wang *et al.* [160] prepared g-C_3N_4 amine-rich mesoporous nanosheets by a thermal stripping method. Due to their large surface areas, abundant mesoporous and high concentration of –NH_2 groups, these nanosheets showed higher CO_2 adsorption and selectivity than pure g-C_3N_4 materials.

CHALLENGES AND PROSPECTS

As global climate change continues to intensify, reducing greenhouse gas emissions has become an important task facing the global community. Carbon neutrality refers to the reduction of greenhouse gas emissions through various measures and, if necessary, the use of carbon sink technologies to reduce the net CO_2 emissions in the atmosphere to zero. In this context, the research and application of photocatalytic CO_2 reduction technology is highly important. Photocatalytic CO_2 reduction converts CO_2 into useful compounds such as CH_4, HCOOH, and CH_3OH. These compounds can be used as fuels or chemicals, thus enabling the resourceful use of CO_2. Compared with conventional fossil fuels, the use of these CO_2 reduction products does not increase CO_2 emissions and thus can significantly reduce the greenhouse gas emissions. Compared with other CO_2 reduction technologies, photocatalytic CO_2 reduction has the

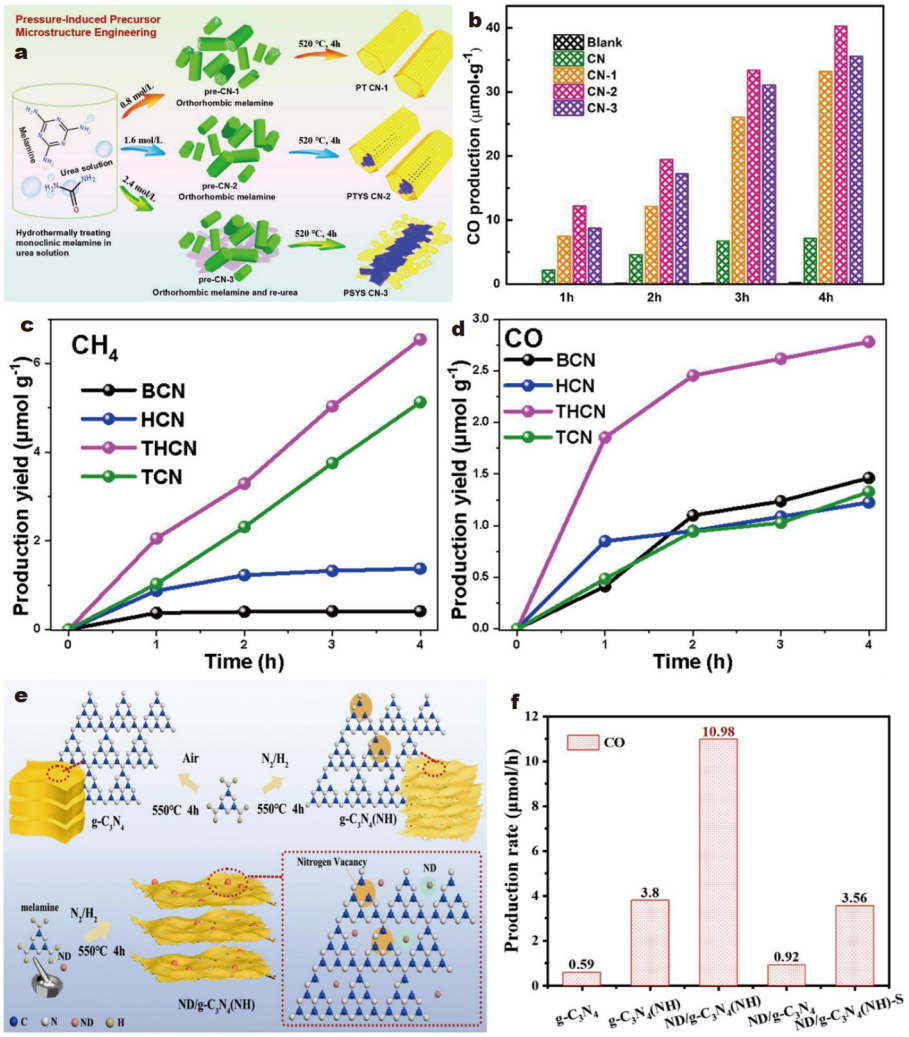

Figure 17 (a) Schematic illustration of the formation of CN-x (x = 1–3). (b) CO production rates over pure CN and CN-x samples. Reprinted with permission from Ref. [157]. Copyright 2019, Elsevier. (c) CH_4 and (d) CO evolutions over BCN, HCN, THCN and TCN under visible light ($\lambda \geqslant 420$ nm). Reprinted with permission from Ref. [158]. Copyright 2021, Elsevier. (e) Preparation processes for ND/g-C_3N_4(NH), g-C_3N_4 (NH) and g-C_3N_4. (f) Comparison of CO production rates for g-C_3N_4, g-C_3N_4 (NH), ND/g-C_3N_4 (NH), ND/g-C_3N_4, and ND/g-C_3N_4 (NH)-S. Reprinted with permission from Ref. [159]. Copyright 2022, Elsevier.

advantages of direct solar energy utilization and relatively simple and low-cost operation. Therefore, photocatalytic CO_2 reduction technology has received much attention. g-C_3N_4 has been studied and applied as an efficient and economical photocatalyst for CO_2 photocatalytic reduction; however, the photocatalytic reduction activity of pristine g-C_3N_4 for CO_2 is not high, and various modulation tools have been applied to enhance the catalytic performance of g-C_3N_4 for CO_2 photocatalytic reduction and achieved good results in the laboratory. Although researchers have made many efforts to enhance the efficiency of g-C_3N_4-based photocatalysts for photocatalytic CO_2 reduction, much research is still needed before they can be applied in practice. Unfortunately, due to the current climate issues and policy regulations, the low efficiency of g-C_3N_4-based photocatalysts for CO_2 reduction needs to be addressed to meet practical needs. To meet these challenges, several suggestions and perspectives for future research are presented below.

(1) Improvement of the adsorption of CO_2: CO_2 adsorption is the first step of the photocatalytic CO_2 reduction reaction, and enhancing the adsorption of CO_2 by a catalyst is beneficial for improving the efficiency of CO_2 reduction. The adsorption of CO_2 can be effectively enhanced by introducing functional groups or ligands that act as Lewis base sites. However, too strong of an adsorption can cause difficulty for the reduction products to desorb and occupy the active sites; thus, the proper adsorption of CO_2 by the catalyst is beneficial for enhancing its photocatalytic reduction efficiency.

(2) Optimization of the use of sacrificial agents: H_2O can be used as a sacrificial agent for the g-C_3N_4 photocatalytic reduction of CO_2 by providing additional electrons and protons and thus promoting the reduction of CO_2. Compared with other sacrificial agents, such as methanol and ethanol, the use of water as a sacrificial agent is more environmentally friendly. In the photocatalytic reduction of CO_2 with H_2O as a sacrificial agent, a competing reaction of hydrogen precipitation and decomposition of H_2O produces oxygen molecules; these processes may cause oxidation reactions with the CO_2 reduction products, leading to a decrease in the selectivity of the reaction. Therefore, more efficient g-C_3N_4-based photocatalysts need to be researched and designed in the future to reduce the dependence on

sacrificial agents.

(3) In-depth investigation of the mechanism of the CO_2 reduction process: the basic principle of g-C_3N_4 photocatalytic CO_2 reduction has been initially studied, but the specific reaction process and especially the mechanism of reduction product generation have not been studied in depth; additionally, there is no systematic understanding of the physicochemical process of photocatalytic CO_2 reduction, which hinders the design of more efficient g-C_3N_4-based photocatalysts. Therefore, to develop g-C_3N_4-based photocatalysts that meet practical needs, a deeper study of the reaction mechanism should be carried out to design synthetic catalysts to ensure the optimal level of catalyst performance in each reaction process.

(4) Improvement of the selectivity of the reduced products: in general, the position of the CB can determine the type of reduced products, and the energy band modulation of g-C_3N_4 by different modulation strategies can be used to select the reduced products. In addition, increasing the mobility of photogenerated carriers is beneficial for enhancing the selectivity of the reduced products. The photogenerated electrons avoid complex migration with holes to the catalyst surface, and a large number of photogenerated electrons accumulate on the catalyst surface, which can effectively improve the reaction rate and increase the selectivity for the reduced products in highly reduced states.

(5) Design of catalysts and processes under practical conditions: the g-C_3N_4-based photocatalysts studied at this stage not only have low photoconversion efficiency to meet the needs of practical applications but also have not yet been tested for stability and reusability in practical applications. In addition, most research has been performed in the laboratory without designing reaction devices to meet actual needs, and the catalytic efficiency of the synthesized catalysts under actual working conditions is not able to be determined. Therefore, the design and optimization of actual reaction devices to improve the catalytic efficiency of catalytic reaction systems will be the focus of future research.

The aim of this review is to provide theoretical support for the applications of g-C_3N_4 photocatalytic CO_2 reduction in a carbon-neutral context and to promote the practical applications of g-C_3N_4 photocatalytic CO_2 reduction and the design of efficient g-C_3N_4-based photocatalysts. In the future, with the joint efforts of scientific researchers worldwide, g-C_3N_4-based high-efficiency photocatalysts will likely be able to meet the practical needs of industrial CO_2 reduction, achieve large-scale CO_2 conversion, reduce CO_2 emissions, and contribute to the global carbon neutrality goal and sustainable development of global energy.

Received 19 January 2024; accepted 26 March 2024; published online 13 May 2024

1 Kohse-Höinghaus K. Combustion, chemistry, and carbon neutrality. Chem Rev, 2023, 123: 5139–5219
2 Wang F, Harindintwali JD, Yuan Z, *et al.* Technologies and perspectives for achieving carbon neutrality. Innovation, 2021, 2: 100180
3 Liu Z, Deng Z, He G, *et al.* Challenges and opportunities for carbon neutrality in China. Nat Rev Earth Environ, 2022, 3: 141–155
4 Zhang B, Zhang J, Zhang F, *et al.* Selenium-doped hierarchically porous carbon nanosheets as an efficient metal-free electrocatalyst for CO_2 reduction. Adv Funct Mater, 2020, 30: 1906194
5 Qiu N, Li J, Wang H, *et al.* Emerging dual-atomic-site catalysts for electrocatalytic CO_2 reduction. Sci China Mater, 2022, 65: 3302–3323
6 Mikkelsen M, Jørgensen M, Krebs FC. The teraton challenge. A review of fixation and transformation of carbon dioxide. Energy Environ Sci, 2010, 3: 43–81
7 Wang J, Fu J, Zhao Z, *et al.* Benefit analysis of multi-approach biomass energy utilization toward carbon neutrality. Innovation, 2023, 4: 100423
8 Zhang N, Long R, Gao C, *et al.* Recent progress on advanced design for photoelectrochemical reduction of CO_2 to fuels. Sci China Mater, 2018, 61: 771–805
9 Liu L, Zhao H, Andino JM, *et al.* Photocatalytic CO_2 reduction with H_2O on TiO_2 nanocrystals: Comparison of anatase, rutile, and brookite polymorphs and exploration of surface chemistry. ACS Catal, 2012, 2: 1817–1828
10 Zhang H, Li Y, Wang J, *et al.* An unprecedent hydride transfer pathway for selective photocatalytic reduction of CO_2 to formic acid on TiO_2. Appl Catal B-Environ, 2021, 284: 119692
11 Ali S, Razzaq A, Kim H, *et al.* Activity, selectivity, and stability of earth-abundant $CuO/Cu_2O/Cu_0$-based photocatalysts toward CO_2 reduction. Chem Eng J, 2022, 429: 131579
12 Chen J, Xiao Y, Wang N, *et al.* Facile synthesis of a Z-scheme CeO_2/C_3N_4 heterojunction with enhanced charge transfer for CO_2 photoreduction. Sci China Mater, 2023, 66: 3165–3175
13 Wang M, Shen M, Jin X, *et al.* Exploring the enhancement effects of hetero-metal doping in CeO_2 on CO_2 photocatalytic reduction performance. Chem Eng J, 2022, 427: 130987
14 Li P, Hu H, Luo G, *et al.* Crystal facet-dependent CO_2 photoreduction over porous ZnO nanocatalysts. ACS Appl Mater Interfaces, 2020, 12: 56039–56048
15 Dong YJ, Jiang Y, Liao JF, *et al.* Construction of a ternary WO_3/$CsPbBr_3$/ZIF-67 heterostructure for enhanced photocatalytic carbon dioxide reduction. Sci China Mater, 2022, 65: 1550–1559
16 Pan YX, You Y, Xin S, *et al.* Photocatalytic CO_2 reduction by carbon-coated indium-oxide nanobelts. J Am Chem Soc, 2017, 139: 4123–4129
17 Zhou Y, Tian Z, Zhao Z, *et al.* High-yield synthesis of ultrathin and uniform Bi_2WO_6 square nanoplates benefitting from photocatalytic reduction of CO_2 into renewable hydrocarbon fuel under visible light. ACS Appl Mater Interfaces, 2011, 3: 3594–3601
18 Chen X, Chen Y, Liu X, *et al.* Boosted charge transfer and photocatalytic CO_2 reduction over sulfur-doped C_3N_4 porous nanosheets with embedded SnS_2-SnO_2 nanojunctions. Sci China Mater, 2022, 65: 400–412
19 Wang Y, Qu Y, Qu B, *et al.* Construction of six-oxygen-coordinated single Ni sites on g-C_3N_4 with boron-oxo species for photocatalytic water-activation-induced CO_2 reduction. Adv Mater, 2021, 33: 2105482
20 Kuang Y, Shang J, Zhu T. Photoactivated graphene oxide to enhance photocatalytic reduction of CO_2. ACS Appl Mater Interfaces, 2020, 12: 3580–3591
21 Cho KM, Kim KH, Park K, *et al.* Amine-functionalized graphene/CdS composite for photocatalytic reduction of CO_2. ACS Catal, 2017, 7: 7064–7069
22 Liang J, Zhang W, Liu Z, *et al.* Tuning metal-free hierarchical boron nitride-like catalyst for enhanced photocatalytic CO_2 reduction activity. ACS Catal, 2022, 12: 12217–12226
23 Sun K, Qian Y, Jiang H. Metal-organic frameworks for photocatalytic water splitting and CO_2 reduction. Angew Chem Int Ed, 2023, 62: e202217565
24 Chen Y, Wang D, Deng X, *et al.* Metal–organic frameworks (MOFs) for photocatalytic CO_2 reduction. Catal Sci Technol, 2017, 7: 4893–4904
25 Dong M, Gu JX, Sun CY, *et al.* Photocatalytic reduction of low-concentration CO_2 by metal–organic frameworks. Chem Commun, 2022, 58: 10114–10126
26 Wang X, Maeda K, Thomas A, *et al.* A metal-free polymeric photocatalyst for hydrogen production from water under visible light. Nat Mater, 2009, 8: 76–80
27 Lu Q, Eid K, Li W, *et al.* Engineering graphitic carbon nitride (g-C_3N_4) for catalytic reduction of CO_2 to fuels and chemicals: Strategy and mechanism. Green Chem, 2021, 23: 5394–5428
28 Ong W, Putri LK, Mohamed AR. Rational design of carbon-based 2D nanostructures for enhanced photocatalytic CO_2 reduction: A di-

mensionality perspective. Chem Eur J, 2020, 26: 9710–9748
29 Höhne N, Gidden MJ, den Elzen M, *et al.* Wave of net zero emission targets opens window to meeting the Paris Agreement. Nat Clim Chang, 2021, 11: 820–822
30 Zhang D, Li Y, Li Y, *et al.* Towards single-atom photocatalysts for future carbon-neutral application. SmartMat, 2022, 3: 417–446
31 Hallegatte S, Rogelj J, Allen M, *et al.* Mapping the climate change challenge. Nat Clim Change, 2016, 6: 663–668
32 Fuglestvedt J, Rogelj J, Millar RJ, *et al.* Implications of possible interpretations of 'greenhouse gas balance' in the Paris Agreement. Phil Trans R Soc A, 2018, 376: 20160445
33 Höhne N, den Elzen M, Rogelj J, *et al.* Emissions: World has four times the work or one-third of the time. Nature, 2020, 579: 25–28
34 Figueres C, Schellnhuber HJ, Whiteman G, *et al.* Three years to safeguard our climate. Nature, 2017, 546: 593–595
35 Levin K, Rich D. Turning points: Trends in countries' reaching peak greenhouse gas emissions over time. World Resources Institute, 2017. https://www.wri.org/research/turning-points-trends-countries-reaching-peak-greenhouse-gas-emissions-over-time
36 Nie H, Kemp R, Fan Y. Investigating the adoption of energy-saving measures in residential sector: The contribution to carbon neutrality of China and Europe. Resources Conservation Recycling, 2023, 190: 106791
37 Lyu X, Yang K, Fang J. Utilization of resources in abandoned coal mines for carbon neutrality. Sci Total Environ, 2022, 822: 153646
38 Kang Z, Liao Q, Zhang Z, *et al.* Carbon neutrality orientates the reform of the steel industry. Nat Mater, 2022, 21: 1094–1098
39 De La Peña L, Guo R, Cao X, *et al.* Accelerating the energy transition to achieve carbon neutrality. Resources Conservation Recycling, 2022, 177: 105957
40 Davis SJ, Lewis NS, Shaner M, *et al.* Net-zero emissions energy systems. Science, 2018, 360: eaas9793
41 Yang X, Nielsen CP, Song S, *et al.* Breaking the hard-to-abate bottleneck in China's path to carbon neutrality with clean hydrogen. Nat Energy, 2022, 7: 955–965
42 Wang F, Hou T, Zhao X, *et al.* Ordered macroporous carbonous frameworks implanted with CdS quantum dots for efficient photocatalytic CO_2 reduction. Adv Mater, 2021, 33: 2102690
43 Li K, Peng B, Peng T. Recent advances in heterogeneous photocatalytic CO_2 conversion to solar fuels. ACS Catal, 2016, 6: 7485–7527
44 Osterloh FE. Photocatalysis *versus* photosynthesis: A sensitivity analysis of devices for solar energy conversion and chemical transformations. ACS Energy Lett, 2017, 2: 445–453
45 Zhou P, Navid IA, Ma Y, *et al.* Solar-to-hydrogen efficiency of more than 9% in photocatalytic water splitting. Nature, 2023, 613: 66–70
46 Inoue T, Fujishima A, Konishi S, *et al.* Photoelectrocatalytic reduction of carbon dioxide in aqueous suspensions of semiconductor powders. Nature, 1979, 277: 637–638
47 Nordin NA, Mohamed MA, Salehmin MNI, *et al.* Photocatalytic active metal–organic framework and its derivatives for solar-driven environmental remediation and renewable energy. Coord Chem Rev, 2022, 468: 214639
48 Mao Y, Wang P, Li L, *et al.* Unravelling the synergy between oxygen vacancies and oxygen substitution in BiO_{2-x} for efficient molecular-oxygen activation. Angew Chem Int Ed, 2020, 59: 3685–3690
49 Liu S, Wang M, He Y, *et al.* Covalent organic frameworks towards photocatalytic applications: Design principles, achievements, and opportunities. Coord Chem Rev, 2023, 475: 214882
50 Sun Z, Wang H, Wu Z, *et al.* g-C_3N_4 based composite photocatalysts for photocatalytic CO_2 reduction. Catal Today, 2018, 300: 160–172
51 Karamian E, Sharifnia S. On the general mechanism of photocatalytic reduction of CO_2. J CO2 Utilization, 2016, 16: 194–203
52 Sun Z, Talreja N, Tao H, *et al.* Catalysis of carbon dioxide photoreduction on nanosheets: Fundamentals and challenges. Angew Chem Int Ed, 2018, 57: 7610–7627
53 Wang Y, Chen E, Tang J. Insight on reaction pathways of photocatalytic CO_2 conversion. ACS Catal, 2022, 12: 7300–7316
54 White JL, Baruch MF, Pander Iii JE, *et al.* Light-driven heterogeneous reduction of carbon dioxide: Photocatalysts and photoelectrodes. Chem Rev, 2015, 115: 12888–12935
55 Hong L, Guo R, Zhang Z, *et al.* Fabrication of porous octahedron-flowerlike microsphere NH_2-UiO-66/$CdIn_2S_4$ heterojunction photocatalyst for enhanced photocatalytic CO_2 reduction. J CO2 Utilization, 2021, 51: 101650
56 Li X, Yu J, Jaroniec M, *et al.* Cocatalysts for selective photoreduction of CO_2 into solar fuels. Chem Rev, 2019, 119: 3962–4179
57 Gong E, Ali S, Hiragond CB, *et al.* Solar fuels: Research and development strategies to accelerate photocatalytic CO_2 conversion into hydrocarbon fuels. Energy Environ Sci, 2022, 15: 880–937
58 Indrakanti VP, Kubicki JD, Schobert HH. Photoinduced activation of CO_2 on Ti-based heterogeneous catalysts: Current state, chemical physics-based insights and outlook. Energy Environ Sci, 2009, 2: 745–758
59 Ji Y, Luo Y. New mechanism for photocatalytic reduction of CO_2 on the anatase TiO_2 (101) surface: The essential role of oxygen vacancy. J Am Chem Soc, 2016, 138: 15896–15902
60 Franklin EC. The ammono carbonic acids. J Am Chem Soc, 1922, 44: 486–509
61 Wang Y, Wang X, Antonietti M. Polymeric graphitic carbon nitride as a heterogeneous organocatalyst: From photochemistry to multipurpose catalysis to sustainable chemistry. Angew Chem Int Ed, 2012, 51: 68–89
62 Pauling L, Sturdivant JH. The structure of cyameluric acid, hydromelonic acid and related substances. Proc Natl Acad Sci USA, 1937, 23: 615–620
63 Teter DM, Hemley RJ. Low-compressibility carbon nitrides. Science, 1996, 271: 53–55
64 Jiang Z, Zhang X, Chen H-, *et al.* Fusiform-shaped g-C_3N_4 capsules with superior photocatalytic activity. Small, 2020, 16: 2003910
65 Li Y, Xu H, Ouyang S, *et al. In situ* surface alkalinized g-C_3N_4 toward enhancement of photocatalytic H_2 evolution under visible-light irradiation. J Mater Chem A, 2016, 4: 2943–2950
66 Fu J, Zhu B, Jiang C, *et al.* Hierarchical porous O-doped g-C_3N_4 with enhanced photocatalytic CO_2 reduction activity. Small, 2017, 13: 1603938
67 Ji H, Chang F, Hu X, *et al.* Photocatalytic degradation of 2,4,6-trichlorophenol over g-C_3N_4 under visible light irradiation. Chem Eng J, 2013, 218: 183–190
68 Wang K, Fu J, Zheng Y. Insights into photocatalytic CO_2 reduction on C_3N_4: Strategy of simultaneous B, K co-doping and enhancement by N vacancies. Appl Catal B-Environ, 2019, 254: 270–282
69 Goettmann F, Thomas A, Antonietti M. Metal-free activation of CO_2 by mesoporous graphitic carbon nitride. Angew Chem Int Ed, 2007, 46: 2717–2720
70 Huang P, Huang J, Pantovich SA, *et al.* Selective CO_2 reduction catalyzed by single cobalt sites on carbon nitride under visible-light irradiation. J Am Chem Soc, 2018, 140: 16042–16047
71 Zhang L, Mao F, Zheng LR, *et al.* Tuning metal catalyst with metal–C_3N_4 interaction for efficient CO_2 electroreduction. ACS Catal, 2018, 8: 11035–11041
72 Zhang G, Zhang J, Zhang M, *et al.* Polycondensation of thiourea into carbon nitride semiconductors as visible light photocatalysts. J Mater Chem, 2012, 22: 8083–8091
73 Xu Y, Gao SP. Band gap of C_3N_4 in the GW approximation. Int J Hydrogen Energy, 2012, 37: 11072–11080
74 Wang X, Blechert S, Antonietti M. Polymeric graphitic carbon nitride for heterogeneous photocatalysis. ACS Catal, 2012, 2: 1596–1606
75 Masih D, Ma Y, Rohani S. Graphitic C_3N_4 based noble-metal-free photocatalyst systems: A review. Appl Catal B-Environ, 2017, 206: 556–588
76 Cao S, Low J, Yu J, *et al.* Polymeric photocatalysts based on graphitic carbon nitride. Adv Mater, 2015, 27: 2150–2176
77 Mamba G, Mishra AK. Graphitic carbon nitride (g-C_3N_4) nanocomposites: A new and exciting generation of visible light driven photocatalysts for environmental pollution remediation. Appl Catal B-Environ, 2016, 198: 347–377
78 Zheng Y, Lin L, Wang B, *et al.* Graphitic carbon nitride polymers toward sustainable photoredox catalysis. Angew Chem Int Ed, 2015,

54: 12868–12884
79 Patnaik S, Sahoo DP, Parida K. Recent advances in anion doped g-C_3N_4 photocatalysts: A review. Carbon, 2021, 172: 682–711
80 Hasija V, Nguyen VH, Kumar A, *et al.* Advanced activation of persulfate by polymeric g-C_3N_4 based photocatalysts for environmental remediation: A review. J Hazard Mater, 2021, 413: 125324
81 Balakrishnan A, Chinthala M. Comprehensive review on advanced reusability of g-C_3N_4 based photocatalysts for the removal of organic pollutants. Chemosphere, 2022, 297: 134190
82 Mishra A, Mehta A, Basu S, *et al.* Graphitic carbon nitride (g–C_3N_4)-based metal-free photocatalysts for water splitting: A review. Carbon, 2019, 149: 693–721
83 Shen H, Peppel T, Strunk J, *et al.* Photocatalytic reduction of CO_2 by metal-free-based materials: Recent advances and future perspective. Sol RRL, 2020, 4: 1900546
84 Chang X, Wang T, Gong J. CO_2 photo-reduction: Insights into CO_2 activation and reaction on surfaces of photocatalysts. Energy Environ Sci, 2016, 9: 2177–2196
85 Du L, Gao B, Tian Q, *et al.* Frustrated Lewis Pairs constructed on 2D amorphous carbon nitride for high-selective photocatalytic CO_2 reduction to CH_4. Sol RRL, 2021, 5: 2100673
86 Zhu B, Zhang L, Xu D, *et al.* Adsorption investigation of CO_2 on g-C_3N_4 surface by DFT calculation. J CO2 Utilization, 2017, 21: 327–335
87 Sun Z, Fischer JMTA, Li Q, *et al.* Enhanced CO_2 photocatalytic reduction on alkali-decorated graphitic carbon nitride. Appl Catal B-Environ, 2017, 216: 146–155
88 Azofra LM, MacFarlane DR, Sun C. A DFT study of planar *vs.* corrugated graphene-like carbon nitride (g-C_3N_4) and its role in the catalytic performance of CO_2 conversion. Phys Chem Chem Phys, 2016, 18: 18507–18514
89 Yu Y, Yan W, Wang X, *et al.* Surface engineering for extremely enhanced charge separation and photocatalytic hydrogen evolution on g-C_3N_4. Adv Mater, 2018, 30: 1705060
90 Chen P, Lei B, Dong X', *et al.* Rare-earth single-atom La–N charge-transfer bridge on carbon nitride for highly efficient and selective photocatalytic CO_2 reduction. ACS Nano, 2020, 14: 15841–15852
91 Xu Y, Jin X, Ge T, *et al.* Realizing efficient CO_2 photoreduction in Bi_3O_4Cl: Constructing van der Waals heterostructure with g-C_3N_4. Chem Eng J, 2021, 409: 128178
92 Ye S, Wang R, Wu MZ, *et al.* A review on g-C_3N_4 for photocatalytic water splitting and CO_2 reduction. Appl Surf Sci, 2015, 358: 15–27
93 Kim B, Kwon D, Baeg J, *et al.* Dual-atom-site Sn-Cu/C_3N_4 photocatalyst selectively produces formaldehyde from CO_2 reduction. Adv Funct Mater, 2023, 33: 2212453
94 Wang K, Li Q, Liu B, *et al.* Sulfur-doped g-C_3N_4 with enhanced photocatalytic CO_2-reduction performance. Appl Catal B-Environ, 2015, 176-177: 44–52
95 Dong G, Zhang L. Porous structure dependent photoreactivity of graphitic carbon nitride under visible light. J Mater Chem, 2012, 22: 1160–1166
96 Xia P, Antonietti M, Zhu B, *et al.* Designing defective crystalline carbon nitride to enable selective CO_2 photoreduction in the gas phase. Adv Funct Mater, 2019, 29: 1900093
97 Niu P, Yang Y, Yu JC, *et al.* Switching the selectivity of the photoreduction reaction of carbon dioxide by controlling the band structure of a g-C_3N_4 photocatalyst. Chem Commun, 2014, 50: 10837–10840
98 Li P, Wang F, Wei S, *et al.* Mechanistic insights into CO_2 reduction on Cu/Mo-loaded two-dimensional g-C_3N_4 (001). Phys Chem Chem Phys, 2017, 19: 4405–4410
99 Zhang X, Pei C, Chang X, *et al.* FeO_6 octahedral distortion activates lattice oxygen in perovskite ferrite for methane partial oxidation coupled with CO_2 splitting. J Am Chem Soc, 2020, 142: 11540–11549
100 Ojha N, Bajpai A, Kumar S. Enhanced and selective photocatalytic reduction of CO_2 by H_2O over strategically doped Fe and Cr into porous boron carbon nitride. Catal Sci Technol, 2020, 10: 2663–2680
101 Wang L, Zang L, Shen F, *et al.* Preparation of Cu modified g-C_3N_4 nanorod bundles for efficiently photocatalytic CO_2 reduction. J Colloid Interface Sci, 2022, 622: 336–346
102 Fu S, Liu X, Ran J, *et al.* CO_2 reduction by single copper atom supported on g-C_3N_4 with asymmetrical active sites. Appl Surf Sci, 2021, 540: 148293
103 Wang Y, Xu Y, Wang Y, *et al.* Synthesis of Mo-doped graphitic carbon nitride catalysts and their photocatalytic activity in the reduction of CO_2 with H_2O. Catal Commun, 2016, 74: 75–79
104 Dong X, Zhang S, Wu H, *et al.* Facile one-pot synthesis of Mg-doped g-C_3N_4 for photocatalytic reduction of CO_2. RSC Adv, 2019, 9: 28894–28901
105 Tang J, Guo R, Pan W, *et al.* Visible light activated photocatalytic behaviour of Eu(III) modified g-C_3N_4 for CO_2 reduction and H_2 evolution. Appl Surf Sci, 2019, 467-468: 206–212
106 Wang S, Zhan J, Chen K, *et al.* Potassium-doped g-C_3N_4 achieving efficient visible-light-driven CO_2 reduction. ACS Sustain Chem Eng, 2020, 8: 8214–8222
107 Jia R, Zhang Y, Yang X. High efficiency photocatalytic CO_2 reduction realized by Ca^{2+} and HDMP group Co-modified graphitic carbon nitride. Int J Hydrogen Energy, 2021, 46: 32893–32903
108 Zhang H, Tang Y, Liu Z, *et al.* Study on optical properties of alkali metal doped g-C_3N_4 and their photocatalytic activity for reduction of CO_2. Chem Phys Lett, 2020, 751: 137467
109 Duan Y, Wang Y, Zhang W, *et al.* Simultaneous CO_2 and H_2O activation *via* integrated Cu single atom and N vacancy dual-site for enhanced CO photo-production. Adv Funct Mater, 2023, 33: 2301729
110 Li J, Li K, Du J, *et al.* Impact of transition metal incorporation on the photocatalytic CO_2 reduction activity of polymeric carbon nitride. J CO2 Utilization, 2022, 64: 102162
111 Liu G, Niu P, Sun C, *et al.* Unique electronic structure induced high photoreactivity of sulfur-doped graphitic C_3N_4. J Am Chem Soc, 2010, 132: 11642–11648
112 Fu J, Liu K, Jiang K, *et al.* Graphitic carbon nitride with dopant induced charge localization for enhanced photoreduction of CO_2 to CH_4. Adv Sci, 2019, 6: 1900796
113 Huang X, Gu W, Hu S, *et al.* Phosphorus-doped inverse opal g-C_3N_4 for efficient and selective CO generation from photocatalytic reduction of CO_2. Catal Sci Technol, 2020, 10: 3694–3700
114 Guo Y, Wang M, Tian J, *et al.* Probing the effect of P-doping in polymeric carbon nitride on CO_2 photocatalytic reduction. Dalton Trans, 2020, 49: 15750–15757
115 Xie W, Li K, Liu XH, *et al.* P-mediated Cu-N_4 sites in carbon nitride realizing CO_2 photoreduction to C_2H_4 with selectivity modulation. Adv Mater, 2023, 35: 2208132
116 Qaraah FA, Mahyoub SA, Hezam A, *et al.* Synergistic effect of hierarchical structure and S-scheme heterojunction over O-doped g-C_3N_4/N-doped Nb_2O_5 for highly efficient photocatalytic CO_2 reduction. Appl Catal B-Environ, 2022, 315: 121585
117 Samanta S, Yadav R, Kumar A, *et al.* Surface modified C, O co-doped polymeric g-C_3N_4 as an efficient photocatalyst for visible light assisted CO_2 reduction and H_2O_2 production. Appl Catal B-Environ, 2019, 259: 118054
118 Ojha N, Bajpai A, Kumar S. Visible light-driven enhanced CO_2 reduction by water over Cu modified S-doped g-C_3N_4. Catal Sci Technol, 2019, 9: 4598–4613
119 Wang Y, Tian Y, Yan L, *et al.* DFT study on sulfur-doped g-C_3N_4 nanosheets as a photocatalyst for CO_2 reduction reaction. J Phys Chem C, 2018, 122: 7712–7719
120 Kumar A, Yadav RK, Park NJ, *et al.* Facile one-pot two-step synthesis of novel *in situ* selenium-doped carbon nitride nanosheet photocatalysts for highly enhanced solar fuel production from CO_2. ACS Appl Nano Mater, 2018, 1: 47–54
121 Kumar S, Gawande MB, Kopp J, *et al.* P- and F-co-doped carbon nitride nanocatalysts for photocatalytic CO_2 reduction and thermocatalytic furanics synthesis from sugars. ChemSusChem, 2020, 13: 5231–5238
122 Wan S, Ou M, Zhong Q, *et al.* Haloid acid induced carbon nitride semiconductors for enhanced photocatalytic H_2 evolution and reduction of CO_2 under visible light. Carbon, 2018, 138: 465–474
123 Liu C, Zhang Y, Dong F, *et al.* Chlorine intercalation in graphitic carbon nitride for efficient photocatalysis. Appl Catal B-Environ, 2017, 203: 465–474

124 Yan P, Ji F, Zhang W, *et al.* Engineering surface bromination in carbon nitride for efficient CO_2 photoconversion to CH_4. J Colloid Interface Sci, 2023, 634: 1005–1013
125 Lan ZA, Zhang G, Wang X. A facile synthesis of Br-modified g-C_3N_4 semiconductors for photoredox water splitting. Appl Catal B-Environ, 2016, 192: 116–125
126 Xia J, Chai L, Tian T, *et al.* CN/iodine-doped CN homojunction powder catalysts with excellent visible-light photocatalytic properties. Powder Tech, 2020, 373: 488–496
127 Arumugam M, Tahir M, Praserthdam P. Effect of nonmetals (B, O, P, and S) doped with porous g-C_3N_4 for improved electron transfer towards photocatalytic CO_2 reduction with water into CH_4. Chemosphere, 2022, 286: 131765
128 Zhang X, Wang L, Du Q, *et al.* Photocatalytic CO_2 reduction over B_4C/C_3N_4 with internal electric field under visible light irradiation. J Colloid Interface Sci, 2016, 464: 89–95
129 Xu Y, You Y, Huang H, *et al.* Bi_4NbO_8Cl {001} nanosheets coupled with g-C_3N_4 as 2D/2D heterojunction for photocatalytic degradation and CO_2 reduction. J Hazard Mater, 2020, 381: 121159
130 Ou M, Tu W, Yin S, *et al.* Amino-assisted anchoring of $CsPbBr_3$ perovskite quantum dots on porous g-C_3N_4 for enhanced photocatalytic CO_2 reduction. Angew Chem Int Ed, 2018, 57: 13570–13574
131 Wang H, Li H, Chen Z, *et al.* TiO_2 modified g-C_3N_4 with enhanced photocatalytic CO_2 reduction performance. Solid State Sci, 2020, 100: 106099
132 Li M, Zhang L, Wu M, *et al.* Mesostructured CeO_2/g-C_3N_4 nanocomposites: Remarkably enhanced photocatalytic activity for CO_2 reduction by mutual component activations. Nano Energy, 2016, 19: 145–155
133 Zhang W, Mohamed AR, Ong W. Z-scheme photocatalytic systems for carbon dioxide reduction: Where are we now? Angew Chem Int Ed, 2020, 59: 22894–22915
134 Jiang Z, Wan W, Li H, *et al.* A hierarchical Z-scheme α-Fe_2O_3/g-C_3N_4 hybrid for enhanced photocatalytic CO_2 reduction. Adv Mater, 2018, 30: 1706108
135 Wang M, Shen M, Zhang L, *et al.* 2D-2D MnO_2/g-C_3N_4 heterojunction photocatalyst: *In-situ* synthesis and enhanced CO_2 reduction activity. Carbon, 2017, 120: 23–31
136 Bhosale R, Jain S, Vinod CP, *et al.* Direct Z-scheme g-C_3N_4/$FeWO_4$ nanocomposite for enhanced and selective photocatalytic CO_2 reduction under visible light. ACS Appl Mater Interfaces, 2019, 11: 6174–6183
137 Xu Q, Zhang L, Cheng B, *et al.* S-scheme heterojunction photocatalyst. Chem, 2020, 6: 1543–1559
138 Li Y, Xia Z, Yang Q, *et al.* Review on g-C_3N_4-based S-scheme heterojunction photocatalysts. J Mater Sci Tech, 2022, 125: 128–144
139 He F, Zhu B, Cheng B, *et al.* 2D/2D/0D TiO_2/C_3N_4/Ti_3C_2 MXene composite S-scheme photocatalyst with enhanced CO_2 reduction activity. Appl Catal B-Environ, 2020, 272: 119006
140 Xie Q, He W, Liu S, *et al.* Bifunctional S-scheme g-C_3N_4/Bi/$BiVO_4$ hybrid photocatalysts toward artificial carbon cycling. Chin J Catal, 2020, 41: 140–153
141 Zhou J, Gao B, Wu D, *et al.* Enhanced photocatalytic activity of lead-free Cs_2TeBr_6/g-C_3N_4 heterojunction photocatalyst and its mechanism. Adv Funct Mater, 2024, 34: 2308411
142 Basyach P, Prajapati PK, Rohman SS, *et al.* Visible light-active ternary heterojunction photocatalyst for efficient CO_2 reduction with simultaneous amine oxidation and sustainable H_2O_2 production. ACS Appl Mater Interfaces, 2023, 15: 914–931
143 Madhusudan P, Shi R, Xiang S, *et al.* Construction of highly efficient Z-scheme $Zn_xCd_{1-x}S$/Au@g-C_3N_4 ternary heterojunction composite for visible-light-driven photocatalytic reduction of CO_2 to solar fuel. Appl Catal B-Environ, 2021, 282: 119600
144 Chen L, Li H, Li H, *et al.* Accelerating photogenerated charge kinetics *via* the g-C_3N_4 Schottky junction for enhanced visible-light-driven CO_2 reduction. Appl Catal B-Environ, 2022, 318: 121863
145 Li HJW, Zhou H, Chen K, *et al.* Metallic MoO_2-modified graphitic carbon nitride boosting photocatalytic CO_2 reduction *via* Schottky junction. Sol RRL, 2020, 4: 1900416
146 Khan J, Sun Y, Han L. A comprehensive review on graphitic carbon nitride for carbon dioxide photoreduction. Small Methods, 2022, 6: 2201013
147 Wang Q, Fang Z, Zhang W, *et al.* High-efficiency g-C_3N_4 based photocatalysts for CO_2 reduction: Modification methods. Adv Fiber Mater, 2022, 4: 342–360
148 Yu J, Wang K, Xiao W, *et al.* Photocatalytic reduction of CO_2 into hydrocarbon solar fuels over g-C_3N_4–Pt nanocomposite photocatalysts. Phys Chem Chem Phys, 2014, 16: 11492–11501
149 Ong WJ, Tan LL, Chai SP, *et al.* Heterojunction engineering of graphitic carbon nitride (g-C_3N_4) *via* Pt loading with improved daylight-induced photocatalytic reduction of carbon dioxide to methane. Dalton Trans, 2015, 44: 1249–1257
150 Li F, Zhou H, Fan J, *et al.* Amine-functionalized graphitic carbon nitride decorated with small-sized Au nanoparticles for photocatalytic CO_2 reduction. J Colloid Interface Sci, 2020, 570: 11–19
151 Li P, Liu L, An W, *et al.* Ultrathin porous g-C_3N_4 nanosheets modified with AuCu alloy nanoparticles and C–C coupling photothermal catalytic reduction of CO_2 to ethanol. Appl Catal B-Environ, 2020, 266: 118618
152 Heng Q, Wang B, Fan X, *et al.* Enhanced photoreduction activity of CO_2 to CO over Ag-loaded mesoporous g-C_3N_4 (MCN) by promoting charge separation and CO_2 adsorption. J Alloys Compd, 2022, 920: 165945
153 Khan I, Chu X, Khan I, *et al.* Synthesis of nanosized Ag-modified 2D/2D hydroxylated g-C_3N_4/TS-1 Z-scheme nanocomposites for efficient photocatalytic CO_2 reduction. Mater Res Bull, 2020, 130: 110926
154 Cao S, Li Y, Zhu B, *et al.* Facet effect of Pd cocatalyst on photocatalytic CO_2 reduction over g-C_3N_4. J Catal, 2017, 349: 208–217
155 Lang Q, Hu W, Zhou P, *et al.* Twin defects engineered Pd cocatalyst on C_3N_4 nanosheets for enhanced photocatalytic performance in CO_2 reduction reaction. Nanotechnology, 2017, 28: 484003
156 Wang Z, Lee H, Chen J, *et al.* Synergistic effects of Pd–Ag bimetals and g-C_3N_4 photocatalysts for selective and efficient conversion of gaseous CO_2. J Power Sources, 2020, 466: 228306
157 Tian N, Xiao K, Zhang Y, *et al.* Reactive sites rich porous tubular yolk-shell g-C_3N_4 *via* precursor recrystallization mediated microstructure engineering for photoreduction. Appl Catal B-Environ, 2019, 253: 196–205
158 Yang B, Zhao J, Yang W, *et al.* A step-by-step synergistic stripping approach toward ultra-thin porous g-C_3N_4 nanosheets with high conduction band position for photocatalystic CO_2 reduction. J Colloid Interface Sci, 2021, 589: 179–186
159 Li X, Li S, Xu J, *et al.* Synergy of nitrogen vacancies and nanodiamond decoration in g-C_3N_4 for boosting CO_2 photoreduction. Appl Surf Sci, 2022, 600: 154199
160 Wang H, Liu G, Hao X, *et al.* Rich –NH_2 mesoporous g-C_3 N_4 nanosheets efficient for cycloaddition of CO_2 to epoxides without solvent and co-catalyst. ChemistrySelect, 2021, 6: 3712–3721

Acknowledgements This work was financially supported by the Ministry of Science and Technology of China as a Key Technology Research and Development Program Project (2023YFC3709001), the Ministry of Education of China as a Discipline Innovation and Intelligence Introduction Project (B17025), and Tianjin Science and Technology Bureau as a Key Science and Technology Supporting Project (S19ZC60133).

Author contributions Zhou Q supervised the project and conceived the idea. Zhan H wrote the draft. Zhou R, Liu K, Ma Z, Wang P, and Zhan S revised the manuscript and provided constructive suggestions. All authors discussed and commented on the manuscript.

Conflict of interest The authors declare that they have no conflict of interest.

Haiyin Zhan is a PhD candidate at the College of Environmental Science and Engineering, Nankai University (China) under the supervision of professor Qixing Zhou. His current research area is the construction of highly-efficient atomic catalysts for Fenton-like reactions.

Qixing Zhou is a distinguished professor of Nankai University (China) and serves at the College of Environmental Science and Engineering. He received his PhD degree in ecology from the Chinese Academy of Sciences and Karlsruhe University (Germany) in 1992. His research interests focus on ecological geochemistry, green advanced materials, and environmental remediation.

碳中和背景下基于g-C_3N_4光催化CO_2还原的研究进展与挑战

展海银[1], 周睿人[2], 刘可望[1], 马志辉[1], 王鹏飞[1], 展思辉[1], 周启星[1*]

摘要 全球变暖对人类的生产生活造成了严重的威胁，已成为当今世界面临的重大挑战之一. 碳中和这一重要举措能够有效缓解全球变暖的进程，在这一背景下光催化CO_2还原可有效减少碳排放且促进碳循环. g-C_3N_4因其制备工艺简单、稳定性高、能带位置适宜以及优异的光催化性能而备受关注. 因此，提高g-C_3N_4光催化CO_2还原效率是当前研究的热点问题. 本文重点探究了碳中和对于全球生态平衡和环境可持续发展的重要性以及在碳中和背景下g-C_3N_4光催化CO_2还原的重要作用和发展前景; 综述了目前解决限制g-C_3N_4光催化CO_2还原瓶颈问题的方法和技术手段. 对g-C_3N_4在光催化CO_2还原领域存在的问题进行讨论，提出了未来的研究方向，并进行展望. 本综述旨在为碳中和背景下基于g-C_3N_4催化剂光催化CO_2还原的应用提供理论支持，为基于g-C_3N_4高效CO_2还原光催化剂的设计提供思路.